

Preparation and Characterization of Alkylcarboxylate-Stabilized-Magnesium
Nanoparticles.

by

(Md. Hafizur Rahman)

A thesis submitted in partial fulfillment of the requirements for the degree of
Master of Philosophy
in Department of Chemistry



Khulna University of Engineering & Technology
Khulna-9203, Bangladesh

October, 2011

Dedicated
to
my beloved parents

Md. Habibur Rahman
&
Anwara Khatun

Declaration

This is to certify that the thesis work entitled "**Preparation and Characterization of Alkylcarboxylate-Stabilized-Magnesium Nanoparticles**" has been carried out by Md. Hafizur Rahman in the Department of Chemistry, Khulna University of Engineering & Technology, Khulna, Bangladesh. The above thesis work or any part of this work has not been submitted anywhere for the award of any degree or diploma.



01.10.2011

Signature of Supervisor







01.10.11

Signature of Candidate

Approval

This is to certify that the thesis work submitted by Md. Hafizur Rahman "**Preparation and Characterization of Alkylcarboxylate-Stabilized-Magnesium Nanoparticles.**" has been approved by the board of examiners for the partial fulfillment of the requirements for the degree of Masters of Philosophy in the Department of Chemistry, Khulna University of Engineering & Technology, Khulna, Bangladesh in October, 2011.

BOARD OF EXAMINERS

1.  01.10.2011
Chairman
(Supervisor)
Prof. Dr. Muhammad Abu Yousuf
Department of Chemistry
Khulna University of Engineering & Technology
Khulna-9203, Bangladesh.
2.  01.10.11
Member
Head
Department of Chemistry
Khulna University of Engineering & Technology
Khulna-9203, Bangladesh.
3.  01/10/11
Member
Dr. Md. Abdul Motin
Associate Professor
Department of Chemistry
Khulna University of Engineering & Technology
Khulna-9203, Bangladesh.
4.  1/10/11
Member
(External)
Prof. Dr. Md. Azizur Rahman
Department of Chemistry
University of Dhaka
Dhaka-1000, Bangladesh.

Abstract

Long chain carboxylate shell stabilized magnesium (Mg) nanoparticles (NPs) were synthesized. In the core-shell type NPs the cores are Mg metal and the shells are long chain carboxylates. Synthesis of magnesium nanoparticles (Mg-NPs) involve: i) preparation of water soluble Na-salts of long chain fatty acids in alcoholic medium followed by ii) temperature controlled reaction with magnesium salts in aqueous medium in presence of suitable surfactant, poly vinyl pyrrolidone (PVP). The synthesis procedure used in this work was originally applied for the fabrication of long chain carboxylate capped magnesium nanoparticles.

Structural and geometrical probabilities of prepared NPs were proposed on the basis of evidences from elemental analysis, optical and spectral studies.

The compositions of the NPs were determined by elemental analysis. The experimental and calculated data for carbon (C), hydrogen (H), oxygen (O) and metal were compared. The presence and percentages of C, H and O revealed the presence of alkyl carboxylates and is proposed that these alkyl carboxylates act as protected shells to the Mg-NPs. From the titration of magnesium laurate, magnesium myristate, magnesium palmitate and magnesium stearate 7.83%, 7.02%, 6.54% and 5.93% Mg were found respectively. These values show that all the substances contain relatively higher amount of Mg than those of the molar ratio. These results exposed metallic Mg in the samples. It is proposed that this metallic Mg may be positioned at the core of the NPs. Melting point (MP) data also provide auspicious evidence about the formation of Mg-NPs.

The Fourier Transform Infrared Spectroscopy (FTIR) spectra provide information about the presence of moisture or adhering free water and/or crystalline water and alkyl carboxylates in the NPs. Broad peak at ~ 3040 to 3520 cm^{-1} appears due to O-H stretching vibrations of hydroxyl ($-\text{OH}$) group. This may be due to the presence of moisture absorbed by the sample or water of crystallization. Two characteristic peaks at ~ 1510 to 1600 cm^{-1} and at ~ 1400 to 1510 cm^{-1} were found and these may be due to C=O stretching and C-O stretching of carboxylates respectively.

Transmission Electron Microscopy (TEM) photographs showed the particles have the dimensions over a range of 25–90 nm. At higher magnifications, the NPs were recognized as spherical or oval in shape in all cases.

The NPs are hygroscopic in nature as they absorbed 8.54–12.22% moisture. The moistures and/or crystallized water are also evidenced by the Differential Thermal Analysis (DTA) and Thermogravimetric Analysis (TGA) of the respective NPs. Both DTA and TGA demonstrated the presence of alkyl carboxylates or organic part in the NPs. The loss of organic parts at higher temperatures also corresponds to the decomposition of the NPs at higher temperature in a normal furnace as investigated by FTIR analysis.

Contents

	Page
CHAPTER I Introduction	1
1.1 Nanoparticle	1
1.2 Surfactant	3
1.3 Lauric Acid	5
1.4 Myristic acid	6
1.5 Palmitic acid	6
1.6 Stearic acid	7
1.7 Magnesium laurate	8
1.8 Magnesium myristate	9
1.9 Magnesium palmitate	9
1.10 Magnesium stearate	9
CHAPTER II Literature Review	11
2.1 Literature Review	11
CHAPTER III Plan of the present work	14
3.1 Plan of the present work	14
CHAPTER IV Experimental	17
4.1 General	17
4.2 Materials	17
4.3 Preparation of magnesium laurate	17
4.4 Preparation of magnesium myristate	18
4.5 Preparation of magnesium palmitate	19
4.6 Preparation of magnesium stearate	20
4.7 Elemental analysis	20
4.8 Determination of Magnesium	21
4.9 Determination of moisture content	21
4.10 Melting point determination	22
4.11 Fourier Transform Infrared analysis	23
4.12 Transmission electron microscope	24
4.13 Thermal Analysis	26

CHAPTER V	Results and Discussions	28
	5.1 General	28
	5.2 Preparation of long chain alkyl carboxylate protected magnesium core-shell NPs	28
	5.3 Determination of Magnesium	31
	5.4 Elemental analysis	32
	5.5 Moisture content	33
	5.6 Melting point	33
	5.7 Fourier Transform Infrared Spectroscopy analyses	34
	5.8 Transmission electron microscopy analyses	52
	5.9 Thermal Analysis	53
TABLE	1.1 The chemical formula of PVP and its physical properties	5
	5.1 The results of elemental analysis of carboxylate protected magnesium NPs	32
	5.2 The moisture content of carboxylate protected magnesium NPs	33
	5.3 Tentative assignment of IR bands of Mg-laurate after heating at 90 °C	36
	5.4 Tentative assignment of IR bands of Mg-laurate after heating at 110 °C	38
	5.5 Tentative assignment of IR bands of Mg-myristate after heating at 90 °C	40
	5.6 Tentative assignment of IR bands of Mg-myristate after heating at 110 °C	42
	5.7 Tentative assignment of IR bands of Mg-palmitate after heating at 90 °C	44
	5.8 Tentative assignment of IR bands of Mg-palmitate after heating at 110 °C	46
	5.9 Tentative assignment of IR bands of Mg-stearate after heating at 90 °C	48
	5.10 Tentative assignment of IR bands of Mg-stearate after heating at 110 °C	50
	5.11 Weight loss recorded at different stages of TGA of Mg-laurate NPs	54
	5.12 Weight loss recorded at different stages of TGA of Mg-myristate NPs	55
	5.13 Weight loss recorded at different stages of TGA of Mg-palmitate NPs	55

	5.14	Weight loss recorded at different stages of TGA of Mg-stearate NPs	56
FIGURE	2.1	Schematic depiction of stearate shell protected silver nanoparticle.	12
	3.1	Schematic representation of synthesis of long chain carboxylates shell protected magnesium nanoparticles.	16
	4.1	Elemental (C, H, O) analyzer	21
	4.2	Furnace for moisture determination	22
	4.3	Melting point apparatus (Ogawa–Seiki)	23
	4.4	FTIR Spectrometer (IR-Prestige-21)	24
	4.5	Transmission electron microscopy (TEM) analyzer	26
	4.6	Thermo Gravimetric Analyzer	27
	5.1	Photograph of synthesized Magnesium laurate, Magnesium myristate, Magnesium palmitate and Magnesium stearate.	29
	5.2	Photograph of Mg-EBT complexes (wine-red) and free EBT (Greenish-blue) at end point.	31
	5.3	FTIR spectrum of Mg-laurate after heating at 90 °C	35
	5.4	FTIR spectrum of Mg-laurate after heating at 110 °C	37
	5.5	FTIR spectrum of Mg-myristate after heating at 90°C	39
	5.6	FTIR spectrum of Mg-myristate after heating at 110°C	41
	5.7	FTIR spectrum of Mg-palmitate after heating at 90°C	43
	5.8	FTIR spectrum of Mg-palmitate after heating at 110°C	45
	5.9	FTIR spectrum of Mg-stearate after heating at 90°C	47
	5.10	FTIR spectrum of Mg-stearate after heating at 110°C	49
	5.11	FTIR spectrum of Mg-NPs after heating at 600 °C for 4 hours	51
	5.12	Transmission electron microscopy images of the prepared NPs.	52
	5.13	Thermal Analysis of Mg-laurate NPs	57
	5.14	Thermal Analysis of Mg-myristate NPs	58
	5.15	Thermal Analysis of Mg-palmitate NPs	59
	5.16	Thermal Analysis of Mg-stearate NPs	60
CHAPTER VI		Conclusion	61
		References	62
		List of Symbols and Abbreviation	70

CHAPTER I

Introduction

1.1 Nanoparticle (NP)

There is no accepted international definition of Nanoparticles (NPs), but one given in the new Publicly Available Specification (PAS) commissioned by the United Kingdom Department of Trade and Industry 71:2005 document is: "The ultrafine particle having one or more dimensions of the order of 100 nm or less". There is a note associated with this definition: "Novel properties that differentiate NPs from the bulk material typically develop at a critical length scale of under 100nm. NPs may or may not exhibit size-related properties that differ significantly from those observed in fine particles or bulk materials [1-2]. Although the size of most molecules would fit into the above outline, individual molecules are usually not referred to as NPs. Nanoclusters have at least one dimension between 1 and 100 nanometers and a narrow size distribution. Nanopowders [3] are agglomerates of ultra fine particles, NPs, or nanoclusters. Nanometer-sized single crystals, or single-domain ultra fine particles, are often referred to as nanocrystals. Nanoparticle research is currently an area of intense scientific interest due to a wide variety of potential applications in biomedical, optical and electronic fields.

There is no strict dividing line between NPs and non-nanoparticles. The size at which materials display different properties to the bulk material is material dependent and can certainly be claimed for many materials much larger in size than 100 nm. Definitions certainly become more difficult for materials that are a very long way from being a sphere, such as carbon nano tubes for example. One of the aims for these materials is to grow them into long tubes, certainly not 'nano' in length, but as they have a diameter in the order of 3 nm for a single walled tube, they have properties that distinguish them from other allotropes of carbon, and hence can be described as "nanomaterial". This sort of nanomaterial has led to the extension of the idea of nanomaterial being considered as such if any one of their structural features is on a scale of less than 100 nm, that cause their properties to be different from that of the bulk material.

NPs are of great scientific interest as they are effectively a bridge between bulk materials and atomic or molecular structures. A bulk material should have constant physical properties regardless of its size, but at the nano-scale size-dependent properties are often observed. Thus, the properties of materials change as their size approaches the nanoscale and as the percentage of atoms at the surface of a material becomes significant. For bulk materials larger than one micrometer (or micron), the percentage of atoms at the surface is insignificant in relation to the number of atoms in the bulk of the material. The interesting and sometimes unexpected properties of NPs are therefore largely due to the large surface area of the material, which dominates the contributions made by the small bulk of the material. NPs often possess unexpected optical properties as they are small enough to confine their electrons and produce quantum effects. For example, gold NPs appear deep red to black in solution. NPs of usually yellow gold and gray silicon are red in color. Other size-dependent property changes include quantum confinement in semiconductor particles, surface plasmon resonance in some metal particles and superparamagnetism in magnetic materials. Ironically, the changes in physical properties are not always desirable. Ferromagnetic materials smaller than 10 nm can switch their magnetization direction using room temperature thermal energy, thus making them unsuitable for memory storage [4].

There are several methods for creating NPs. Many of these nanomaterial's are made directly as dry powders, and it is a common myth that these powders will stay in the same state when stored. In fact, they will rapidly aggregate through a solid bridging mechanism in as little as a few seconds. If the NPs need to be kept separate, then they must be prepared and stored in a liquid medium designed to facilitate sufficient interparticle repulsion forces to prevent aggregation.

Scientists have taken to naming their particles after the real world shapes that they might represent. Nanospheres [5], nanoreefs [6], nanoboxes [7] and more have appeared in the literature. These morphologies sometimes arise spontaneously as an effect of a templating or directing agent present in the synthesis such as miscellar emulsions or anodized alumina pores, or from the innate crystallographic growth patterns of the materials themselves [8]. Some of these morphologies may serve a purpose, such as long carbon nanotubes being

used to bridge an electrical junction, or just a scientific curiosity like the stars shown at right. At the small end of the size range, nanoparticles are often referred to as clusters. Spheres, rods, fibers, and cups are just a few of the shapes that have been grown. The study of fine particles is called micromeritics.

Nanoparticle characterization is necessary to establish understanding and control of NP synthesis and applications. Characterization is done by using a variety of different techniques, mainly drawn from materials science. Common techniques are transmission electron microscopy (TEM) Scanning electron microscopy, atomic force microscopy, Dynamic light scattering, X-ray photoelectron spectroscopy, Powder X-ray diffraction, Fourier transform infrared spectroscopy (FTIR), Ultraviolet-visible spectroscopy, dual and nuclear magnetic resonance (NMR).

The field of NP research covers a wide range of interests in the fields of chemistry, Physics and materials science. Control of the Nano scale morphology enables precise control of the properties of the end product. Particle size, morphology and composition can be manipulated to produce materials of different properties. NPs have wide applications in many fields, such as in medicine, electronics, environment, energy, space, food, consumer products, sensors, molecular manufacturing, that means almost everywhere.

1.2 Surfactant

Surfactants are compounds that lower the surface tension of a liquid, the interfacial tension between two liquids, or that between a liquid and a solid. Surfactants may act as detergents, wetting agents, emulsifiers, foaming agents, dispersants and applications such as cleaning, cosmetics, environmental remediation, etc.

Surfactants are usually organic compounds that are amphiphilic, meaning they contain both hydrophobic groups (tails) and hydrophilic groups (heads). Therefore, a surfactant molecule contains both a water insoluble (oil soluble) component and a water soluble component. Surfactant molecules will migrate to the water surface, where the insoluble hydrophobic group may extend out of the bulk water phase, either into the air or, if water is mixed with oil, into the oil phase, while the water soluble head group remains in the water phase. This alignment and aggregation of surfactant molecules at the surface acts to alter the surface

properties of water at the water/air or water/oil interface. Because air is not hydrophilic, surfactants are also foaming agents to varying degrees. Completely non-polar solvents known as degreasers can also remove hydrophobic contaminants, but lacking polar elements may not dissolve in water.

Surfactants reduce the surface tension of water by adsorbing at the liquid-gas interface. They also reduce the interfacial tension their tails form a core that can encapsulate an oil droplet, and their (ionic/polar) heads form an outer shell that maintains favorable contact with water. When surfactants assemble in oil, the aggregate is referred to as a reverse micelle. In a reverse micelle, the heads are in the core and the tails maintain favorable contact with oil.

Surfactants from natural origin (vegetable or animal) are known as oleo-chemicals and are derived from sources such as palm oil or tallow. Surfactants from synthetic origin are known as petro-chemicals and are derived from petroleum. Surfactants are classified into four primary groups; anionic, cationic, non-ionic, and zwitterionic (dual charge).

Thermodynamics of the surfactant systems are of great importance, theoretically and practically. This is because surfactant systems represent systems between ordered and disordered states of matter. Surfactant solutions may contain an ordered phase (micelles) and a disordered phase (free surfactant molecules and/or ions in the solution). They have a vital role to play in preventing the re-deposition of soils like greasy, oily stains and particulate dirt on the surface or fabric from which they have just been removed. This works by electrostatic interactions and steric hindrance. Anionic surfactants are adsorbed on both the surface of the dirt which is dispersed in the detergent solution, and the fabric surface. This creates a negative charge on both surfaces, causing electrostatic repulsions. This repulsion prevents the soil from re-depositing on the fabric. In the presence of hardness, however, this mechanism acts like a 'bridge' between the suspended soil and the fabric. This is another reason why hardness sequestrants (a chemical that promotes Ca/Mg sequestration) are often used in detergents. Surfactants play important role in controlling rate, sizes and shapes of NPs. In this research poly vinyl Pyrrolidone (PVP) was used as surfactant. The chemical formula of PVP and its physical properties are listed in Table 1.1.

Table 1.1: The chemical formula of PVP and its physical properties

Property	Data
Chemical Name	Polyvinyl Pyrrolidone
Chemical formula	$(C_6H_9NO)_n$
Formula weight	about 40 000
Solubility	Soluble in water, in ethanol and in chloroform; insoluble in ether
pH	3.0 - 7.0 (5% soln)
Relative viscosity	Between 1.188 and 1.325
Total ash	Not more than 0.02%

1.3 Lauric Acid

Lauric acid, also called dodecanoic acid is a common saturated fatty acid with the molecular formula $CH_3(CH_2)_{10}COOH$. Molar mass of acid is 200.32 and density is 0.8801 g/cm^3 . The melting point and boiling point of lauric acid are $43.2 \text{ }^\circ\text{C}$ and $298.9 \text{ }^\circ\text{C}$ respectively. It is the main acid in coconut oil and in palm kernel oil, and is believed to have antimicrobial properties. It is a white, powder solid with a faint odor of bay oil or soap. Lauric acid is inexpensive, has a long shelf-life, and is non-toxic and safe to handle. Thus, it is often used in laboratory investigations of freezing-point depression. It is a solid at room temperature but melts easily in boiling water, so liquid lauric acid can be treated with various solutes and used to determine their molecular masses. Lauric acid, although slightly irritating to mucous membranes, has a very low toxicity and so is used in many soaps and shampoos. Sodium lauryl sulfate is the most common lauric acid derived compound used for this purpose. Because lauric acid has a non-polar hydrocarbon tail and a polar carboxylic acid head, it can interact with polar solvents (the most important being water) as well as fats, allowing water to dissolve fats. This accounts for the abilities of shampoos to remove grease from hair. Fatty acids are a carboxylic acid with a long unbranched aliphatic tail (chain), which is either saturated or unsaturated. Fatty acids derived from natural fats and oils may be assumed to

have at least 8 carbon atoms. Most of the natural fatty acids have an even number of carbon atoms, because their biosynthesis involves acetyl-CoA, a coenzyme carrying a two-carbon-atom group. Current experiments have suggested that lauric acid could be a solution for teenage acne [9-10].

1.4 Myristic acid

The molecular formula of myristic acid is $\text{CH}_3(\text{CH}_2)_{12}\text{COOH}$. Its nomenclature according to the International Union of Pure and Applied Chemistry or IUPAC is tetradecanoic acid. It is a common saturated fatty acid with myristic acid is named after the nutmeg *Myristica fragrans*. The CAS number of myristic acid is 544-63-8 and the PubChem number is 11005. Molar mass of acid is 228.37 and density is 0.8622 g/cm^3 . The melting point and boiling point of myristic acid are $54.4 \text{ }^\circ\text{C}$ and $250.5 \text{ }^\circ\text{C}$ respectively at 100 mmHg. A myristate is a salt or ester of myristic acid. Nutmeg butter is 75% trimyristin, the triglyceride of myristic acid. Besides nutmeg myristic acid is also found in palm kernel oil, coconut oil, butter fat and is a minor component of many other animal fats [11]. It is also found in spermacetin, the crystallized fraction of oil from the sperm whale. Myristic acid is also commonly added co-transnationally to the penultimate, nitrogen-terminus, glycine in receptor associated kinases to confer the membrane localization of the enzyme. The myristic acid has a sufficiently high hydrophobicity to become incorporated into the fatty acyl core of the phospholipid bilayer of the plasma membrane of the eukaryotic cell. In this way, myristic acid acts as a lipid anchor in biomembranes. The ester isopropyl myristate is used in cosmetic and topical medicinal preparations where good absorption through the skin is desired. Reduction of myristic acid yields myristyl aldehyde and myristyl alcohol.

1.5 Palmitic acid

Molecular formula of palmitic acid is $\text{CH}_3(\text{CH}_2)_{14}\text{COOH}$. Its nomenclature according to IUPAC, is hexadecanoic acid. The CAS number of Palmitic Acid is 57-10-3 and the PubChem number is 985. Molar mass of acid is 256.42 and density is 0.853 g/cm^3 . The melting point of Palmitic acid is $62.9 \text{ }^\circ\text{C}$ and boiling point of Palmitic acid is $351\text{-}352 \text{ }^\circ\text{C}$ at 100 mmHg. Palmitic acid is one of the most common saturated fatty acids found in animals

and plants. As its name indicates, it is a major component of the oil from palm trees (palm oil and palm kernel oil). Palmitic acid is the first fatty acid produced during lipogenesis (fatty acid synthesis) and from which longer fatty acids can be produced. Palmitic acid is a fatty acid, a type of carboxylic acid which has a long aliphatic tail, which is unbranched and either saturated or unsaturated. If fatty acids are derived from natural fats or oils, they will have at least 8 carbon atoms. Most fatty acids derived from natural sources have an even number of atoms of carbon. The most common palmitic acid sources are the oils from palm trees, like palm oil, coconut oil and palm kernel oil. As mentioned earlier, the name for the fatty acid is derived from the French term for the pith (substance found in vascular plants) of the palm tree. Butter, milk, meat and cheese are also good sources of palmitic acid.

The most widely known use of palmitic acid is that it is an essential ingredient in soap making. During the Second World War, palmitic acid was used after being combined with naphtha, the most volatile part of liquid hydrocarbons, to form napalm, which is a gelling agent that is used in defense operations. About the intake of palmitic acid, researchers are still debating over its effects. According to the World Health Organization, consumption of palmitic acid can increase the chances of occurrence of cardiovascular diseases. There is a contradictory study that says, intake of palmitic acid has no such effect. Palmitic acid derivatives are used in different anti-psychotic medicines, especially in the treatment of schizophrenia.

1.6 Stearic acid

Stearic acid is one of the saturated fatty acid with the formal IUPAC name octadecanoic acid. Its name comes from the Greek word stéar (genitive:stéatos), which means tallow. It is a waxy solid, and chemical formula is $\text{CH}_3(\text{CH}_2)_{16}\text{COOH}$. Molar mass of stearic acid is 284.48 and density is 0.847 g/cm^3 at $70 \text{ }^\circ\text{C}$. Melting point and boiling point of stearic acid are $70 \text{ }^\circ\text{C}$ and $383 \text{ }^\circ\text{C}$ respectively. Stearic acid occurs in many animal and vegetable fats and oils, but it is more common in animal fat than vegetable fat. The important exceptions are cocoa butter and shea butter whose fatty acids consist of 28–45% stearic acid [12]. Stearic acid is prepared by treating animal fat with water at a high pressure and temperature, leading to the hydrolysis of triglycerides. It can also be obtained from the hydrogenation of some unsaturated vegetable oils. Stearic acid undergoes the typical reactions of saturated

carboxylic acids, notably reduction to stearyl alcohol, and esterification with a range of alcohols. They are heated and mixed with caustic potash or caustic soda.

Stearic acid is useful as an ingredient in making candles, plastics, dietary supplements, oil pastels and for softening rubber [13]. It is used to harden soaps, particularly those made with vegetable oil. Stearic acid is also used as a parting compound when making plaster castings from a plaster piece mold or waste mold and when making the mold from shellacked clay original. In this use, powdered stearic acid is dissolved in water and the solution is brushed onto the surface to be parted after casting. This reacts with the calcium in the plaster to form a thin layer of calcium stearate which functions as a release agent. Esters of stearic acid with ethylene glycol, glycol stearate and glycol distearate, are used to produce a pearly effect in shampoos, soaps, and other cosmetic products. It is used along with simple sugar or corn syrup as a hardener in candies. It is used with zinc as zinc stearate as fanning powder for cards to deliver smooth fanning motion. Stearic acid is one of the most commonly used lubricants during injection molding and pressing of ceramic powders [14]. Stearic acid is less likely to be incorporated into cholesterol esters. In epidemiologic and clinical studies stearic acid is associated with low density lipoprotein, lowered cholesterol in comparison with other saturated fatty acids [15]. These findings may indicate that stearic acid is less unhealthy than other saturated fatty acids.

1.7 Magnesium laurate

Magnesium laurate is the magnesium salt of dodecanoic acid, is a white substance which is solid at room temperature. It has the chemical formula $C_{24}H_{46}MgO_4$ or $Mg(C_{12}H_{23}O_2)_2$. Molecular mass of magnesium laurate is 422.93. It has faint fatty odor. Its color is white; vapor pressure is 0.000661 mm/Hg at 25 °C. Melting point and boiling point are 150.4 °C and 521.81 °C at 760 mmHg respectively. The solubility in water is very less, i.e., 0.0001354 mg/L at 25 °C but completely soluble in ethanol.

Magnesium laurate is a green, healthy and safe material. It is treated as non-toxic chemical, have no adverse health effects. It can be used as food additive and functions as binders, emulsifiers, and anticaking agents.

1.8 Magnesium myristate

Magnesium myristate is the magnesium salt of tetradecanoic acid, is a white substance which is solid at room temperature. It has the chemical formula $C_{28}H_{54}MgO_4$ or $Mg(C_{14}H_{27}O_2)_2$. Molecular mass of magnesium myristate is 479.04. It has faint fatty odor. Its color is white, melting point is 131.6 °C and boiling point is 319.6°C at 760 mmHg. It is insoluble in water and ether but slightly soluble in benzene.

Magnesium myristate is a mineral that has strong absorbent properties and some disinfecting properties. It contributes the following noticeable aspects to cosmetics: adhesion, free flow, slip, rub resistance, lubricity, shear resistant treatment, pressibility, surface smoothness, and water repellency, cost effective, mass-market pressed powders, liquid make-ups, mascaras according to research. It also exhibits a moist softness, improved adhesion characteristics, and good hydrophobicity. Magnesium myristate treated pigments can frequently be used to replace untreated materials in existing pressed powder formulations with only a few minor adjustments to reduce binder content. The resulting product may display improved slip, spreadability and wear over the original without compromising the integrity of the tablet. Magnesium myristate is also more economical than other cosmetic adhesives.

1.9 Magnesium palmitate

Magnesium palmitate, also called magnesium salt of hexadecanoic acid, is a white substance which is solid at room temperature. It has the chemical formula $C_{32}H_{62}MgO_4$ or $Mg(C_{16}H_{31}O_2)_2$. Molecular mass of magnesium palmitate is 535.15. It has faint fatty odor. Its vapor pressure is 0.000032 mm/Hg at 25 °C. It is insoluble in water and ether but slightly soluble in alcohol.

Magnesium palmitate is also healthy and safe material. It is treated as non-toxic chemical, has no adverse health effects. It can be used as binders, emulsifiers, and anticaking agents.

1.10 Magnesium stearate

Magnesium stearate, also called magnesium salt of octadecanoic acid, is a white substance which is solid at room temperature. It has the chemical formula $C_{36}H_{70}MgO_4$ or

$\text{Mg}(\text{C}_{18}\text{H}_{35}\text{O}_2)_2$. Molecular mass of magnesium stearate is 591.27. Its odor is slight, color is white, melting point is $88\text{ }^\circ\text{C}$ and density is $1.02\text{g}/\text{cm}^3$. It is insoluble in water and ether but slightly soluble in benzene.

Magnesium stearate is manufactured from both animal and vegetable oils. Some nutritional supplements specify that the magnesium stearate used is sourced from vegetables. When produced by soap and hard water, magnesium stearate and calcium stearate both form a white solid insoluble in water, and are collectively known as 'soap scum'.

Magnesium stearate is generally considered safe for human consumption at levels below 2500 kg per day [16]. It is often used as a diluent [17] in the manufacture of medical tablets, capsules and powders [18]. In this regard, the substance is also useful, because it has lubricating properties, preventing ingredients from sticking to manufacturing equipment during the compression of chemical powders into solid tablets; magnesium stearate is the most commonly used lubricant for tablets [19]. Studies have shown that magnesium stearate may affect the release time of the active ingredients in tablets etc. but not that it reduces the over-all bioavailability of those ingredients [20]. Magnesium stearate is also used to bind sugar in hard candies and is a common ingredient in baby formulas. In pure powder form, the substance can be a dust explosion hazard, although this issue is effectively insignificant beyond the manufacturing plants using it.

CHAPTER II

Literature Review

2.1 Literature Review

The synthesis of nanoparticles has received considerable attention and a lot of different synthetic procedures have been described to obtain NPs in different sizes, shapes, and dispersion media (either aqueous or non-aqueous). Controlling the size, shape and structure of NPs is technologically important because of the strong relation between these parameters and the resulting properties, such as the interaction with light, which is valuable for many applications of NPs [21–24]. These properties, which cannot be observed for the bulk metal, have been applied to catalysis [25], electronics [26], high-density information storage [27], photoluminescence, and electroluminescence devices [28]. The highly potential usage of metal nanoparticles has stimulated development of the preparation techniques for nanoparticles, which include electrolysis [29–31], biochemical methods [32–34], gas condensation [35], laser ablation of metal plate [36], sol–gel techniques [37, 38], sonochemical deposition [39], nanostructured templates [40–42], and thermal decompositions [43–47]. Surface of silver nanoparticles is necessarily protected with some kinds of surfactants against aggregation in solution or stabilization in precipitate form. Surfactants for silver nanoparticles are reportedly, 3-mercaptopropionic acid [48], polyphenylpyrrole [49], dodecanethiol [50], the hydrogenterminated silicon [51], iodide [52], fatty acids [45–47], citrate [53, 54], and ethylenediaminetetraacetic acid [51, 55]. It is worthwhile noting that arbitrary combination of a technique and a surfactant is not successful. A successful example is fatty acid-coated silver nanoparticles by means of thermal decomposition [45–47, 56, 57]. This combination is fascinating in that it can lead to a mass production by a wet process and low temperature heating. Thermal decomposition of silver alkylcarboxylates at 250 °C [45–47], has produced nearly mono-dispersed particles with nanometer size. These particles exhibited the surface plasmon spectra similar to the spectra for thiol-stabilized silver nanoparticles [45]. The silver stearate nanoparticle has been

proved to be composed by a silver core and a silver stearate shell [56], as is illustrated in figure 2.1. The shell plays a part in protecting the particles against aggregation

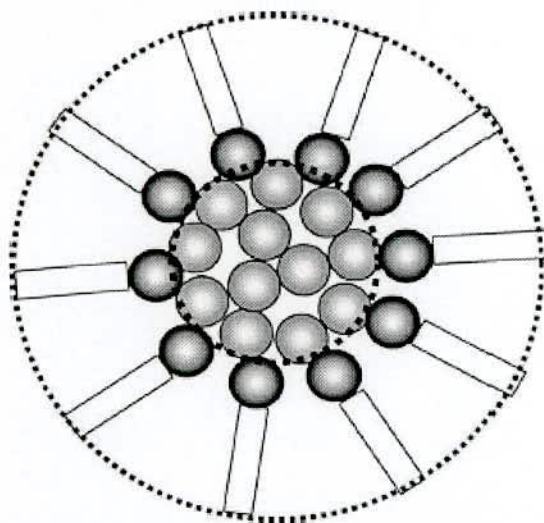


Figure 2.1: Schematic depiction of stearate shell protected silver nanoparticle.

like a surfactant [56, 57]. Aqueous gold nanoparticles dispersions are the most common especially for biomedical and biological applications. The simplest method of preparation is based on the reduction of aqueous hydrogen tetrachloroaurate solution by trisodium citrate. In this method, citrate anions have a dual function; in the beginning they act as the reducing agent to reduce Au^{+3} to Au^0 . Later they also act as a stabilizing agent for the nanoparticle dispersion by forming a charged layer of citrate anions on the surface of the formed particles [58]. The mechanism of citrate reduction of gold chloride salts to form gold nanoparticles occurs through a multi-step process [59]. The further growth of the nanoparticles is dependent on the ratios of the reactants, temperature and also the stirring rate, and can therefore be used to control the sizes of the obtained particles [60]. The finally obtained particles then possess a surface consisting of excess of citrate, which renders the particles negatively charged and consequently well disperses in the reaction medium. Subsequently, the surface of the citrate-stabilized gold nanoparticles demands a further protection in order to increase the aggregation stability. For this task, self-assembled monolayers (SAMs) on gold provide a versatile tool to protect and stabilize gold nanoparticles by separating the metal core from the surrounding environment, in order to prevent occurring particle growth

and reversible agglomeration [61]. Poly(ethylene glycol) (PEG) derivatives here have been widely used to coat and stabilize gold nanoparticles, because they are hydrophilic, water soluble, biocompatible and also resistant to unspecific protein adsorption due to the steric stabilization of the PEG chains [62–65]. Many different research papers describe the useful application of similarly functionalized gold nanoparticles. Yoshimoto et al. [66], for example, reported the preparation of PEGylated gold nanoparticles, which were intended to be used as high-performance photothermal agents in photothermal therapy. They appear to be non-toxic and enable higher and longer imaging times than currently possible using standard iodine-based agents [67]. A very recent study showed the successful use of antibody-conjugated PEGylated gold nanoparticles to label human cancer tissue that has been surgically resected from patients. Since the used gold nanoparticle-antibody conjugates are effectively stabilized by heterofunctional PEG molecules, they are highly stable under the biological conditions and unbound particles can be rinsed away quantitatively when the incubated tissue doesn't contain the targeted antigen [68].

Magnesium stearate is used extensively as a powder lubricant in tablet formulations and commercially available batches vary in both chemical [69–71] and physical character [72] and have an unpredictable effect on formulations [73–74]. However, in many studies involving magnesium stearate and palmitate, but little or no description of the physical and chemical nature is given. To the best of our knowledge, nothing has been described about magnesium stearate, palmitate, myristate and laurate nanoparticles. This anticipation leads us to prepare and characterize magnesium alkylcarboxylates-coated nanoparticles, at the aim of understanding the stability of the magnesium nanoparticles.

CHAPTER III

Plan of the present work

3.1 Plan of the present work

The development of the ability to connect the large surface area-to-volume ratios and the unique surface properties of nanoparticles especially is a major driving force in both fundamental research and practical applications of NPs. It is this size range over which metal particles undergo a transition from atomic to metallic properties. There are two major challenges for developing nanometer-sized particles 1) the control of sizes and compositions and 2) The prevention of the aggregation propensity of nanoscale metal to the bulk. The recent exploration of core-shell type nanoparticles, which can be broadly defined as core and shell of different matters in close interaction, including inorganic/organic, inorganic/inorganic, organic/organic, or inorganic/biological combinations [77–79], provides fascinating pathways to address these challenges. The use of such nanoparticles as building blocks towards catalytic materials takes advantage of diverse attributes, including size monodispersity, processibility, solubility, stability, self-assembly capability, and unique optical, electronic, magnetic, and chemical/biological properties.

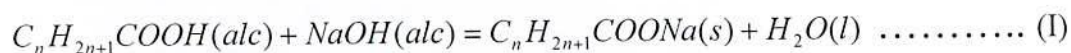
Co-precipitation, deposition-precipitation, ion-exchange, impregnation, and successive reduction and calcination methods have been widely used [80–82] for naked metal NPs preparation. Physical methods, such as proton irradiation [83], laser ablation [84] and vacuum vapor deposition [83], are capable of producing of metal nanoparticles, however; the quality of produced particles is not as high as chemically synthesized ones. These physical methods usually require expensive vacuum systems to generate plasmas. In recent studies [56, 58] long chain fatty acid based silver nanoparticle was reported. Surface of silver nanoparticles is necessarily protected with some kinds of surfactants against aggregation in solution or stabilization in precipitate form. Surfactants for silver nanoparticles are reportedly, 3-mercaptopropionic acid [48], polyphenylpyrrole [49], dodecanethiol [50], the hydrogenterminated silicon [51], iodide [52], fatty acids [45–47], citrate [53, 54], and

ethylenediaminetetraacetic acid [51, 55]. It is worthwhile noting that arbitrary combination of a technique and a surfactant is not successful. A successful example is fatty acid-coated silver nanoparticles by means of thermal decomposition [45–47, 56, 57]. This combination is fascinating in that it can lead to a mass production by a wet process and low temperature heating. Thermal decomposition of silver alkylcarboxylates at 250 °C [45–47], has produced nearly mono-dispersed particles with nanometer size. Therefore, not only surfactant but also temperature is dynamic force of synthesis of polymer-stabilized-metal nanoparticle.

In this thesis, we focused on the study:

- ❖ To synthesize core-shell nanoparticles, encapsulated with long chain alkyl carboxylate shells.
- ❖ To use suitable surfactant for prevention of the aggregation propensity of NP to the bulk.
- ❖ To control temperature for getting the desired NPs of technological applications.
- ❖ To characterize the synthesized NPs.

Keeping above vision the present research is devotedly involved in synthesis long chain alkyl carboxylate protected magnesium core-shell nanoparticles. The shell i.e., long chain alkyl carboxylates in this investigation are stearate, palmitate, myristate and laurate from stearic acid, palmitic acid, myristic acid and lauric acid respectively. The core is magnesium metal. Substitution of hydrogen of the mentioned fatty acids by magnesium may produce long chain alkyl carboxylate protected magnesium nanoparticles such as magnesium stearate, magnesium palmitate, magnesium myristate and magnesium laurate. For this purpose, water soluble sodium salts of the long chain fatty acids were synthesized followed by the reaction with water soluble magnesium salts to attain the desired products. The general steps of the reaction may be



Here, n = 11, 13, 15 and 17.

To avoid the aggregation required amount of surfactant, PVP was supplemented in reaction (II) and apposite temperature was conserved for the production of NPs. The total reaction scheme can be shown by the figure 3.1.

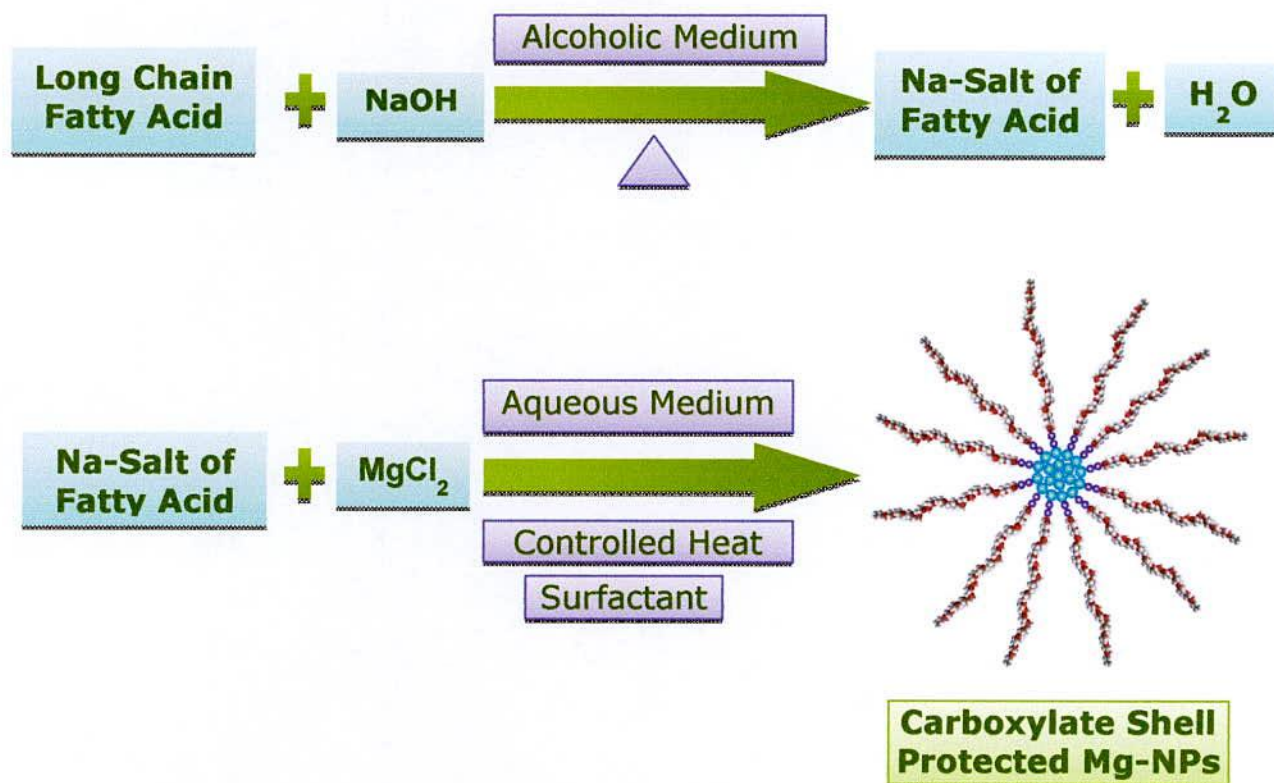


Figure 3.1: Schematic representation of synthesis of long chain carboxylates shell protected magnesium nanoparticles.

A series of experiments like, melting point determination, elemental analyses, FTIR analyses, were performed to find out the purity of the synthesized products. Several attempts have been made to characterize the products of the reaction and to elucidate the NPs morphology.

CHAPTER IV

Experimental

4.1 General

During the course of the present work, a number of techniques were involved which were in general standard ones, constant efforts for attaining the ideal conditions for the experiments were always attempted.

The glass apparatus used in the experimental assembly were ground joint type, which was usually of quick-fit type. Some were normal glass ware. The thoroughly cleaned glass pieces were dried in electric oven.

Hygroscopic and reactive materials were usually stored under closed conditions in a vacuum desiccator and were manipulated out of contact with atmosphere by devising suitable guarding arrangement.

4.2 Materials

Lauric acid, myristic acid, palmitic acid and stearic acid were obtained from Loba Chemie Pvt. Ltd., India. All these acids were analytical grade and were 99.8% pure. High performance liquid chromatography (HPLC) grade ethanol was collected from E-Merck, Germany. Extra pure magnesium chloride and sodium hydroxide were received from E-Merck, Germany. Chemicals and reagents were of analytical grade and were used without further purification.

4.3 Preparation of magnesium laurate

The preparation process was done in two steps. In the first step, sodium laurate was prepared. 3.0 g of lauric acid was dissolved in 100 mL of ethanol in a 250 mL beaker. About 0.60g of sodium hydroxide was dissolved in 100 mL of ethanol in another 250 mL beaker. These two solutions were taken in a 300 mL beaker and heated at 60 °C for about 3 hours. A white precipitate of sodium laurate was formed. The reaction was taken to be complete when a stable pH of 9-10 was attained. Then the precipitate was separated by filtration by Whatman No. 1 filter paper. To remove the unreacted reagents it was then washed by ethanol several

times. The adhering ethanol was evaporated by vacuum heating the precipitate at 80 °C in a vacuum oven and almost pure sodium laurate was obtained.

In the second step, magnesium laurate was synthesized from prepared sodium laurate. 0.75 g of magnesium chloride was dissolved in 50 mL of water in a 250 mL beaker. Prepared sodium laurate was dissolved in 200 mL of water in a 500 mL beaker. To resist agglomeration of NPs 1.2% (w/v) PVP was used. Then it was heated to the reaction temperature. Magnesium chloride solution was added drop wise very vigilantly over a period of 70 minutes. A white precipitate of magnesium laurate nanoparticle was produced in the reaction system. The reaction system was kept at heated condition for about six hours to complete the reaction. This product was cooled for about 12 hours, after which the precipitate was filtered and washed with distilled warm water, finally with ethanol to remove any unreacted lauric acid, magnesium chloride or sodium hydroxide. The resulting white nano powder of magnesium laurate was dried in an oven to constant weight at 110 °C.

4.4 Preparation of magnesium myristate

The preparation process was done in two steps. In the first step, sodium myristate was prepared. 3.0 g of lauric acid was dissolved in 100 mL of ethanol in a 250 mL beaker. About 0.55 g of sodium hydroxide was dissolved in 100 mL of ethanol in another 250 mL beaker. These two solutions were taken in a 300 mL beaker and heated at 60 °C for about 3 hours. A white precipitate of sodium myristate was formed. The reaction was taken to be complete when a stable pH of 9-10 was attained. Then the precipitate was separated by filtration by Whatman No. 1 filter paper. To remove the unreacted reagents it was then washed by ethanol several times. The adhering ethanol was evaporated by vacuum heating the precipitate at 80 °C in a vacuum oven and almost pure sodium myristate was obtained.

In the second step, magnesium myristate was synthesized from prepared sodium myristate. 0.65 g of magnesium chloride was dissolved in 50 mL of water in a 250 mL beaker. Prepared sodium myristate was dissolved in 200 mL of water in a 500 mL beaker. To resist agglomeration of NPs 1.2% (w/v) PVP was used. Then it was heated to the reaction

temperature. Magnesium chloride solution was drop wise added very vigilantly over a period of 70 minutes. A white precipitate of magnesium myristate nanoparticle was produced in the reaction system. The reaction system was kept at heated condition for about six hours to complete the reaction. This product was cooled for about 12 hours, after which the precipitate was filtered and washed with distilled warm water, finally with ethanol to remove any unreacted myristic acid, magnesium chloride or sodium hydroxide. The resulting white nano powder of magnesium myristate was dried in an oven to constant weight at 110 °C.

4.5 Preparation of magnesium palmitate

The preparation process was done in two steps. In the first step, sodium palmitate was prepared. 3.0 g of palmitic acid was dissolved in 100 mL of ethanol in a 250 mL beaker. About 0.50 g of sodium hydroxide was dissolved in 100 mL of ethanol in another 250 mL beaker. These two solutions were taken in a 300 mL beaker and heated at 60 °C for about 3 hours. A white precipitate of sodium palmitate was formed. The reaction was taken to be complete when a stable pH of 9-10 was attained. Then the precipitate was separated by filtration by Whatman No. 1 filter paper. To remove the unreacted reagents it was then washed by ethanol several times. The adhering ethanol was evaporated by vacuum heating the precipitate at 80 °C in a vacuum oven and almost pure sodium palmitate was obtained.

In the second step, magnesium palmitate was synthesized from prepared sodium palmitate. 0.58 g of magnesium chloride was dissolved in 50 mL of water in a 250 mL beaker. Prepared sodium myristate was dissolved in 200 mL of water in a 500 mL beaker. To resist agglomeration of NPs 1.2% (w/v) PVP was used. Then it was heated to the reaction temperature. Magnesium chloride solution was added drop wise very vigilantly over a period of 70 min. A white precipitate of magnesium palmitate nanoparticle was produced in the reaction system. The reaction system was kept at heated condition for about six hours to complete the reaction. This product was cooled for about 12 hours, after which the precipitate was filtered and washed with distilled warm water, finally with ethanol to remove any unreacted palmitic acid, magnesium chloride or sodium hydroxide. The resulting white nano powder of magnesium palmitate was dried in a vacuum oven to constant weight at 80 °C.

4.6 Preparation of magnesium stearate

The preparation process was done in two steps. In the first step, sodium stearate was prepared. 3.0 g of stearic acid was dissolved in 100 mL of ethanol in a 250 mL beaker. About 0.45 g of sodium hydroxide was dissolved in 100 mL of ethanol in another 250 mL beaker. These two solutions were taken in a 300 mL beaker and heated at 60 °C for about 3 hours. A white precipitate of sodium stearate was formed. The reaction was taken to be complete when a stable pH of 9-10 was attained. Then the precipitate was separated by filtration by Whatman No. 1 filter paper. To remove the unreacted reagents it was then washed by ethanol several times. The adhering ethanol was evaporated by vacuum heating the precipitate at 80 °C in a vacuum oven and almost pure sodium stearate was obtained.

In the second step, magnesium stearate was synthesized from prepared sodium stearate. 0.52 g of magnesium chloride was dissolved in 50 mL of water in a 250 mL beaker. Prepared sodium stearate was dissolved in 200 mL of water in a 500 mL beaker. To resist agglomeration of NPs 1.2% (w/v) PVP was used. Then it was heated to the reaction temperature. Magnesium chloride solution was added drop wise very vigilantly over a period of 70 min. A white precipitate of magnesium stearate nanoparticle was produced in the reaction system. The reaction system was kept at heated condition for about six hours to complete the reaction. This product was cooled for about 12 hours, after which the precipitate was filtered and washed with distilled warm water, successively with ethanol to remove any unreacted stearic acid, magnesium chloride or sodium hydroxide. The resulting white nano powder of magnesium stearate was dried in a vacuum oven to constant weight at 65 °C.

4.7 Elemental analysis

Elemental analysis is an experiment that determines the amount (typically a weight percent) of an element in a compound. Just as there are many different elements, there are many different experimental methods for determining elemental composition. The most common type of elemental analysis is for carbon, hydrogen, oxygen and nitrogen. This type of analysis is especially useful for organic compounds (compounds containing carbon-carbon bonds).

The elemental analysis of a compound enables one to determine the empirical formula of the compound. The empirical formula is the formula for a compound that contains the smallest set of integer ratios for the elements in the compound that gives the correct elemental composition by mass. The elemental analysis was done by the PerkinElmer 2400 in the laboratory of Helmholtz Center of Environment in Germany.



Figure 4.1: Elemental (CHO) analyzer

4.8 Determination of Magnesium

0.95 g of the disodium ethylenediaminetetraacetic acid (EDTA) salt was dissolved into a 250 mL volumetric flask to prepare 0.01 N solution. 10.0 mL solution of which the Mg is to be determined was taken into a conical flask. Approximately 15.0 mL of pH 10 buffer and 25.0 mL of distilled water was added to the flask. A few crystals of Eriochrome Black - T indicator was added, a wine-red color was produced. The solution was then titrated with standardized EDTA solution and a clear greenish-blue color solution was obtained at the end point. Then amount of Mg was calculated.

4.9 Determination of moisture content

2.0 g of the sample was taken in a crucible. Then the crucible was placed in a preheated muffle furnace (Lenton Thermal Designs Ltd, made in England) and the temperature was

maintained 105 °C for several hours. Then it was transferred to a desiccator to cool it. The heating and cooling system was repeated to get constant weight. The moisture content was determined from:

$$\text{Moisture content} = \left[\frac{(A - B)}{A} \right] \times 100$$

Where, A = Weight of original sample
 B = Weight of dried sample

Each experiment was performed five times and their mean value was taken.

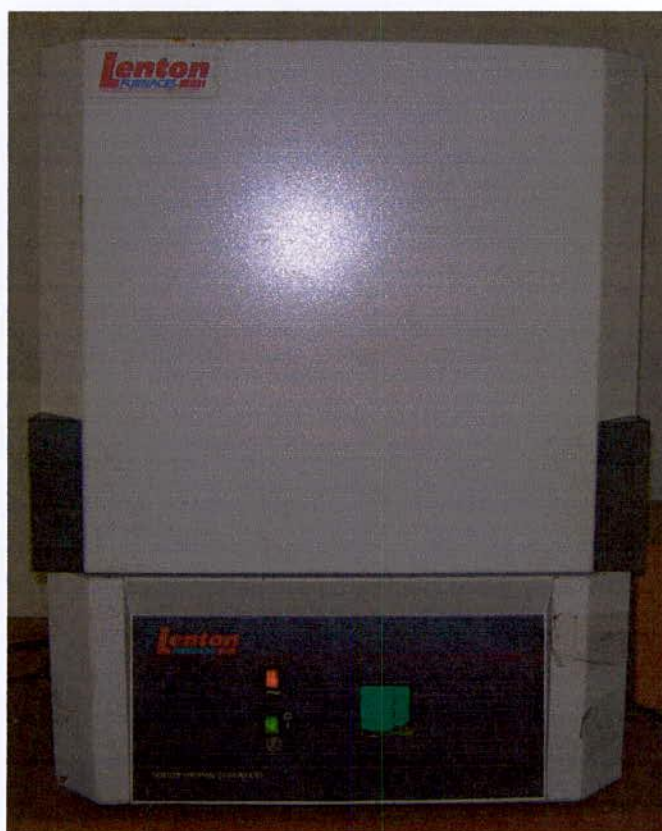


Figure 4.2: Furnace for moisture determination

4.10 Melting point determination

Coarse and nonhomogeneous samples were crushed into a fine powder in an agate mortar. MP capillaries were dried fully then samples were loaded in homogeneous and powdered form. This makes the heat transfer into the sample more efficient and reproducible, and also

enhances the overall reflectivity of the sample for easier automated detection of the melt. The samples were filled in a capillary tube with the open end of the capillary was pressed gently into the substance several times. The powder is then pushed to the bottom of the tube by repeatedly pounding the bottom of the capillary against a hard surface. A sample packing wire was used at the end of compact the sample and to obtain improve the reproducibility of the measurements. A sample height between 2.0 mm and 3.0 mm is maintained for each experiment. The sample tubes are loaded into MP apparatus (Ogawa–Seiki) by inserting the sample loaded capillary into the sample position slot located on top of the instrument. The temperature of the samples continues to rise at the user-specified ramping rate until a user-specified stop temperature is reached. Automated visual observations of the MP were recorded by melting point apparatus (Ogawa–Seiki) at inorganic laboratory of Dhaka University.



Figure 4.3: Melting point apparatus (Ogawa–Seiki)

4.11 Fourier Transform Infrared analysis

Fourier transform spectroscopy is a technique for collecting spectra and measuring the temporal coherence of its radiation source, applying time-domain measurements of electromagnetic or other types of radiation. It can be utilized to various spectroscopy methods including infrared spectroscopy. Molecular vibrations can be analyzed by infrared spectroscopy (IR spectroscopy), and since for each molecule these vibrations occur at specified frequencies, the spectra can be interpreted by checking the peaks with the IR database to determine the chemical structure of the sample. There are two instrumental variations of IR spectroscopy; the older disperse one, in which prisms are used to disperse the IR radiation, and the more recent version, that is, FTIR that uses the principle of

interferometry. All of the FTIR spectra in this work were taken with a FTIR spectrophotometer (IR Prestige-21 Shimadzu, Japan). The infrared spectra were recorded for the wavenumbers in the range of 400-4000 cm^{-1} with a resolution of 4 cm^{-1} . The spectra for the investigated materials were obtained by mixing and grinding a small amount of materials with dry and pure KBr. Thorough mixing and grinding of the materials were accomplished in a agate mortar. The powder mixture thus obtained was then compressed in a metal holder under a pressure of 8–10 tons to make pellet. The pellet was then placed in the path of the IR beam in the spectrometer for measurements.

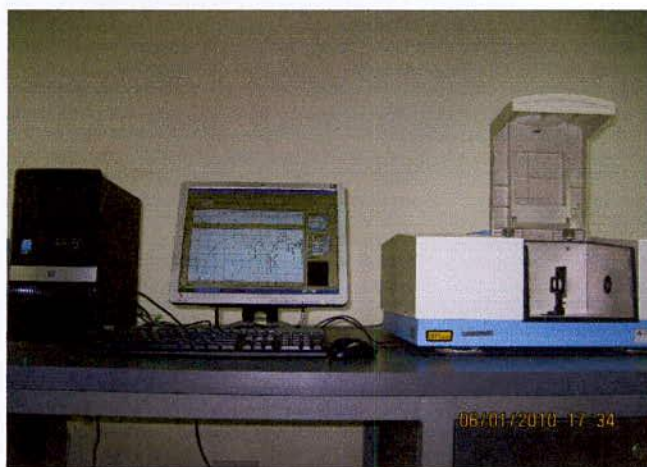


Figure 4.4: FTIR Spectrometer (IR-Prestige-21)

4.12: Transmission electron microscopy

TEM is a microscopy technique whereby a beam of electrons is transmitted through an ultra-thin specimen, interacting with the specimen as it passes through. An image is formed from the interaction of the electrons transmitted through the specimen; the image is magnified and focused onto an imaging device, such as a fluorescent screen, on a layer of photographic film, or to be detected by a sensor such as a camera.

TEMs are capable of imaging at a significantly higher resolution than light microscopes, owing to the small de Broglie wavelength of electrons. This enables the instrument's user to examine fine detail—even as small as a single column of atoms, which is tens of thousands times smaller than the smallest resolvable object in a light microscope. TEM forms a major analysis method in a range of scientific fields, in both physical and biological sciences. TEMs find application in cancer research, virology, materials science as well as pollution, nanotechnology, and semiconductor research.

At smaller magnifications TEM image contrast is due to absorption of electrons in the material, due to the thickness and composition of the material. At higher magnifications complex wave interactions modulate the intensity of the image, requiring expert analysis of observed images. Alternate modes of use allow for the TEM to observe modulations in chemical identity, crystal orientation, electronic structure and sample induced electron phase shift as well as the regular absorption based imaging.

Imaging methods in TEM utilize the information contained in the electron waves exiting from the sample to form an image. The projector lenses allow for the correct positioning of this electron wave distribution onto the viewing system. The observed intensity of the image, I , assuming sufficiently high quality of imaging device, can be approximated as proportional to the time-average amplitude of the electron wave functions, where the wave which form the exit beam is denoted by Ψ [75].

$$I(x) = \frac{k}{t_1 - t_0} \int_{t_0}^{t_1} \Psi \Psi^* dt$$

Different imaging methods therefore attempt to modify the electron waves exiting the sample in a form that is useful to obtain information with regards to the sample, or beam itself. From the previous equation, it can be deduced that the observed image depends not only on the amplitude of beam, but also on the phase of the electrons, although phase effects may often be ignored at lower magnifications. Higher resolution imaging requires thinner samples and higher energies of incident electrons. Therefore the sample can no longer be considered to be absorbing electrons, via a Beer's law effect, rather the sample can be modeled as an object that does not change the amplitude of the incoming electron wave function. Rather the sample modifies the phase of the incoming wave; this model is known as a pure phase object, for sufficiently thin specimens phase effects dominate the image, complicating analysis of the observed intensities [75]. For example, to improve the contrast in the image the TEM may be operated at a slight defocus to enhance contrast, owing to convolution by the contrast transfer function of the TEM [76], which would normally decrease contrast if the sample was not a weak phase object. For the samples TEM was operated at an accelerating voltage of 80 kV with a LaB6 source. For morphological analysis the TEM was operated in bright field mode. For analytical investigations the TEM was operated in the scanning mode. A

diffraction grating replica was used to calibrate the images. NPs suspensions in toluene were drop cast onto 300-mesh copper grids and then were air-dried before viewing. Size and morphological analysis of the NPs was done manually on no less than 200 particles.



Figure 4.5: Transmission electron microscopy (TEM) analyzer

4.13 Thermal Analysis

Thermo gravimetric analysis (TGA) and Differential scanning Analysis (DTA) are techniques by which the thermal behavior of substances is characterized. Whenever a substance is heated it expands and the variation in the extent of expansion with increasing temperature is dependent on the bond energy/ crystal structure etc., and hence on the type of material. Thus, the changes in crystal structure, coefficient of thermal expansion and melting, can be studied with the help of DTA which measures the relative expansion/ contraction between a sample and the standard with varying temperature. TGA on the other hand, measures the change in mass of the sample with varying temperature there by indicating the onset, midpoint and completion of a reaction such as oxidation, decomposition, compound formation etc. Thus oxidation, decomposition, chemical reactions, the calorific value, heat of reaction, specific heat etc. can be calculated.

The thermal analyses were obtained on the TA Instruments 2100 thermal analysis system. Samples in the range of 16–30 mg but accurately weighed case to case were taken into an Aluminum made crucible of which the volume was 100 μL . Then it was inserted in the furnace. The crucible was hermetically sealed, and a pinhole was punched into the crucible lid. The use of the pinhole allows for pressure release, but still ensures that the thermal reactions proceed under controlled conditions. The total atmosphere was air. For either measurement, the samples were heated at a rate of 10 $^{\circ}\text{C}/\text{min}$. The heating temperature was 20–475 $^{\circ}\text{C}$. Both DTA and TGA were carried out on samples previously equilibrated at 20 $^{\circ}\text{C}$ below 45% relative humidity.



Figure 4.6 : Thermo Gravimetric Analyzer

CHAPTER V

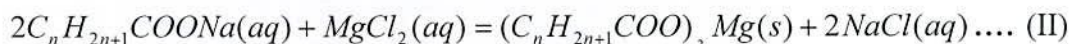
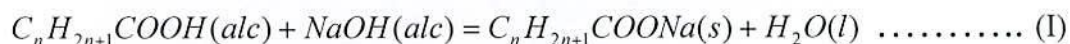
Results and Discussions

5.1 General

During the course of the present work, a number of techniques were involved which were in general standard ones, constant efforts for attaining the ideal conditions for the experiments were always attempted. Several attempts have been made to set the optimum conditions of preparing long chain fatty acids shell protected Mg-NPs. A series of investigations like, melting point determination, FTIR analysis, moisture content, TEM analysis, thermal analysis etc. were accomplished to confirm the NPs synthesis and their characterization.

5.2 Preparation of long chain alkyl carboxylate protected magnesium core-shell NPs:

Long chain carboxylate, e.g., laurate, myristate, palmitate or stearate stabilized magnesium NPs were synthesized by two step reaction. At first, long chain fatty acids, such as, lauric acid, myristic acid, palmitic acid or stearic acid reacted with sodium hydroxide to produce water soluble sodium salt of the corresponding acid in alcoholic medium. Later this sodium salt, like sodium laurate, sodium myristate, sodium palmitate or sodium stearate reacted with magnesium chloride in presence of PVP surfactant in aqueous medium and produced laurate, myristate, palmitate or stearate stabilized magnesium NPs through heat controlled reaction.



Here, in case of $(C_nH_{2n+1}COO)_2Mg(s)$; $n = 11$ ~magnesium laurate, 13~magnesium myristate, 15~magnesium palmitate and 17~magnesium stearate. Stabilizing the surface by capping it with a shell of organic molecules can lead to form NPs of controllable size, shape and surface properties. Figure -5.1 shows the photograph of carboxylate stabilized magnesium NPs. From the figure it is seen that the products are very fine solids. It is very



Figure 5.1: Photograph of synthesized Magnesium laurate, Magnesium myristate, Magnesium palmitate and Magnesium stearate.

common phenomenon the shell, while enhancing stability against aggregation of NPs [45–47, 56, 57]. It is well-known that an important challenge in any nanofabrication technique is agglomeration. Agglomeration is an irreversible fusing of individual nanoparticles when they are free to contact each other, which leads to formation of fractal aggregates. This phenomenon should be avoided since most of desirable properties of nanoparticles are destroyed after they become agglomerated. One way to impede agglomeration is by providing a steric barrier by introducing a capping molecule to the surface of the nanoparticle before agglomeration can occur. Well-capped nanoparticles are no longer at risk of agglomeration. In preparation of carboxylate stabilized magnesium NPs 1.2% (w/v) PVP was used to resist agglomeration. Surfactants are amphiphilic compounds, meaning that they have a hydrophilic head and a hydrophobic tail. It is thought that the head produces an image charge on the nanoparticle surface, while the hydrophobic tail provides the steric repulsion to stop agglomeration. The mechanism may be described through the formation of emulsion. An emulsion may be formed when an amphiphilic molecule (e.g., surfactant) is introduced to the system. The hydrocarbon parts are essentially immiscible; however, upon the addition of surfactant, the interfacial tension between them reduces and they become emulsified. As was mentioned before, the surfactant has an amphiphilic molecular structure: a hydrophilic head group, which prefers aqueous environments and a hydrophobic tail group, which prefers organic environments. This characteristic structure enables the surfactant to reside in both polar and non-polar liquids in the system.

Another typical phenomenon during nanoparticle synthesis is flocculation. Capped nanoparticles may get fairly close to each other and form clusters, called “flocs”. In this case, individual nanoparticles are insulated from each other by the capping agent, but they are close enough to be considered as a group. “Flocculents” or “flocs” can be re-dispersed, while agglomerated nanoparticles are permanently fused and can no longer be separated. [80–82]. Flocculation can be applied to sediment nanoparticles in colloidal solutions. In our system heating and aeration may ensure proper role for flocculation.

All the prepared NPs were white in color. They were insoluble in aqueous medium but soluble in ethanol, pyridine, benzene, dimethyl sulfoxide (DMSO), dimethyl formamide (DMF) and carbon tetra chloride.

The NPs floated on the water surface but sunk in toluene, indicating that they should have a hydrophobic surface. The NPs were protective enough against the oxidation by concentrated nitric acid and air. They showed so high electric resistance that a multimeter was out of range for powder samples, although they include Mg metal as the core. These properties are ascribed to the enclosure of the magnesium core with the hydrophobic alkyl carboxylate chains, as is illustrated in figure 3.1.

5.3 Determination of Magnesium

Eriochrome Black-T (EBT) exists as a wine-red complex when Mg^{2+} is present in solution at $pH = 10$. When the EDTA has chelated all the Mg^{2+} present in solution, the EBT indicator (free and uncomplexed to Mg^{2+}) will be greenish-blue as shown in figure 5.2. This color change marks the endpoint. From the titration of magnesium laurate, magnesium myristate, magnesium palmitate and magnesium stearate we got 7.83%, 7.02%, 6.54% and 5.93% Mg

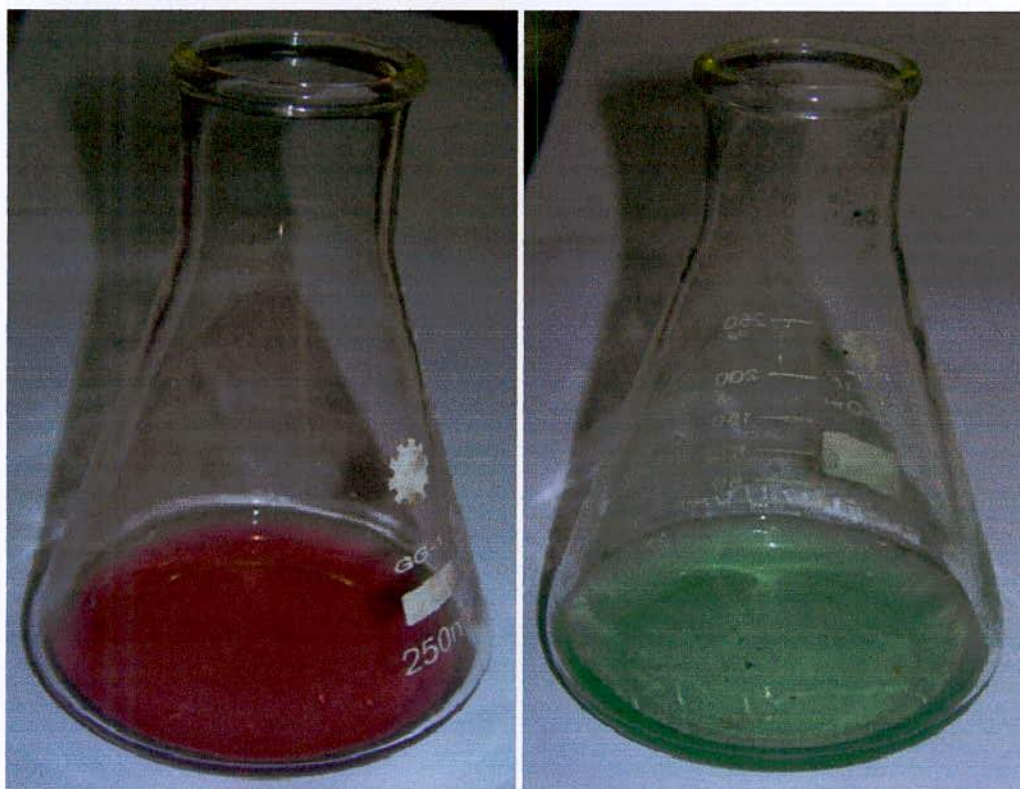


Figure 5.2: Photograph of Mg-EBT complexes (wine-red) and free EBT (Greenish-blue) at end point.

respectively. These values show that all the substances contain relatively higher amount of Mg than those of the molar ratio. From this result it may be presumed or expected that there are some portions of metallic Mg persist in the samples. This extra metallic Mg may act as core of the carboxylate shell protected Mg-NPs as reported in [56, 57, 83–85] for carboxylate shell protected silver-NPs and core-shell Cu NPs.

5.4 Elemental analysis:

Elemental analyses of the carboxylate protected magnesium NPs showed the molar ratio of C:H:O consistent results with those of carboxylates. The results of elemental analysis have been shown in table 5.1. It is seen that in case of magnesium laurate NPs the ratio C:H:O = 5.79:10.03:1.00 is very close to the molar ratio of laurate, $C_{12}H_{23}O_2$ (12:23:2). Similarly for Mg-myristate NPs, Mg-palmitate NPs and Mg-stearate NPs the experimental values of C:H:O are 6.32:12.04:1.00; 7.48:14.87:1.00 and 8.17:15.37:1.00 respectively while the theoretical molar ratio for the myristate $C_{14}H_{27}O_2$, palmitate $C_{16}H_{31}O_2$ and stearate $C_{18}H_{35}O_2$ are 14:27:2, 16:31:2 and 18:35:2 respectively. The elemental analyses evidently show that there are protected shells of carboxylates persist upon the NPs.

Table 5.1: The results of elemental analysis of carboxylate protected magnesium NPs

Name of the samples	Amount of the different samples obtained by elemental analyses (g)			Obtained ratio C: H: O	Theoretical ratio C: H: O	Amount of the sample analyzed (g)
	C	H	O			
Mg-laurate NPs	0.4988	0.0720	0.1148	5.79:10.03:1.00	12:23:2	0.780
Mg-myristate NPs	0.3802	0.0603	0.0801	6.32:12.04:1.00	14:27:2	0.632
Mg-palmitate NPs	0.3120	0.0517	0.0556	7.48:14.87:1.00	16:31:2	0.530
Mg-stearate NPs	0.318	0.0498	0.0519	8.17:15.37:1.00	18:35:2	0.483

5.5 Moisture content

The moisture content data show that all the samples, magnesium laurate, magnesium myristate, magnesium palmitate and magnesium stearate contain significant amount moisture content from a molar consideration as shown in table 5.2. These results correlate the experimental results of FTIR and thermal analysis. The moistures are indicated by the sharpness of the respective DTA endotherms and TGA sample weight loss over a small temperature range. Also, the infra-red spectra showed a broad band from 3200 to 3700 cm^{-1} , the characteristic band of bound moisture.

It is reported earlier that the shape, surface area and moisture content of magnesium stearate, palmitate, myristate and laurate are clearly influenced by manufacturing conditions [86].

Table 5.2: The moisture content of carboxylate protected magnesium NPs

Name of the samples	Moisture content by heating the sample at 105 °C in a furnace (% w/w)	Moisture content obtained by TGA (% w/w)
Mg-laurate NPs	8.54	7.96
Mg-myristate NPs	9.49	8.66
Mg-palmitate NPs	11.07	10.98
Mg-stearate NPs	12.22	11.85

5.6 Melting point

The MP of a substance is the temperature at which the material changes from a solid to a liquid state. Pure crystalline substances have a clear, sharply defined melting point. During the melting process, all of the energy added to a substance is consumed as heat of fusion, and the temperature remains constant. A pure substance melts at a precisely defined temperature, characteristic of every crystalline substance and dependent only on pressure (though the pressure dependency is generally considered insignificant). Determining the MP is a simple and fast method used in many diverse areas of chemistry to obtain a first impression of the purity of a substance. This is because even small quantities of impurities change the melting point, or at least clearly enlarge its melting range.

The MP of dried, moisture free sample of magnesium laurate, magnesium myristate, magnesium palmitate and magnesium stearate NPs were determined. No sharp melting point was observed. Instead MP ranges were obtained in all cases. We found the results for magnesium laurate, magnesium myristate, magnesium palmitate and magnesium stearate NPs were 144.4–149.0, 127.6–132.3, 108.1–111.8 and 84.0–87.3 °C respectively. These results are different from the pure magnesium laurate, magnesium myristate, magnesium palmitate and magnesium stearate or even from pure Mg metal. Melting points of the pure magnesium laurate, magnesium myristate, magnesium palmitate and magnesium stearate are 150.1, 131, 112 and 88 °C respectively. The melting point of pure Mg metal is 649 °C. The melting point ranges indicate that the prepared substances are not pure one. The reduction of melting point may be due to the incorporation of very tiny percentage of Mg into the particles although it has very high melting point.

5.7 FTIR analyses

The FTIR spectra of Mg-carboxylate NPs are shown in Figure – 5.3 to 5.10. The vibrational frequencies and their tentative band assignments are listed in Table 5.3 to 5.10. In all the samples a very broad peak at ~3040 to 3520 cm^{-1} appears due to O-H stretching vibrations of –OH group. This may be due to the presence of moisture absorbed by the sample or water of crystallization [86]. It is seen that when the substances are heated at 110 °C the peaks of O–H at the mentioned region were weaken. This may be due to the removal of moisture which demonstrates the substances are hygroscopic. Two strong sharp peaks at ~2860 to ~3040 cm^{-1} are due to asymmetric and symmetric stretching vibrations of C-H group. Two characteristic peaks at ~1510 to 1600 cm^{-1} and at ~1400 to 1510 cm^{-1} were found and these may be due to C=O stretching and C-O stretching of carboxylates respectively. The -CH₂-bending vibrations found at ~1250 to 1320 cm^{-1} as well as –CH₃ bending vibrations appear at ~1080 to 1150 cm^{-1} . The IR data clearly represent the presence of alkyl carboxylates in the samples. Samples were heated at 600 °C for about four hours. It is seen that about 90% weight has been lost. IR spectrum of rest of the samples has been shown in figure 5.11. No characteristic peak was found.

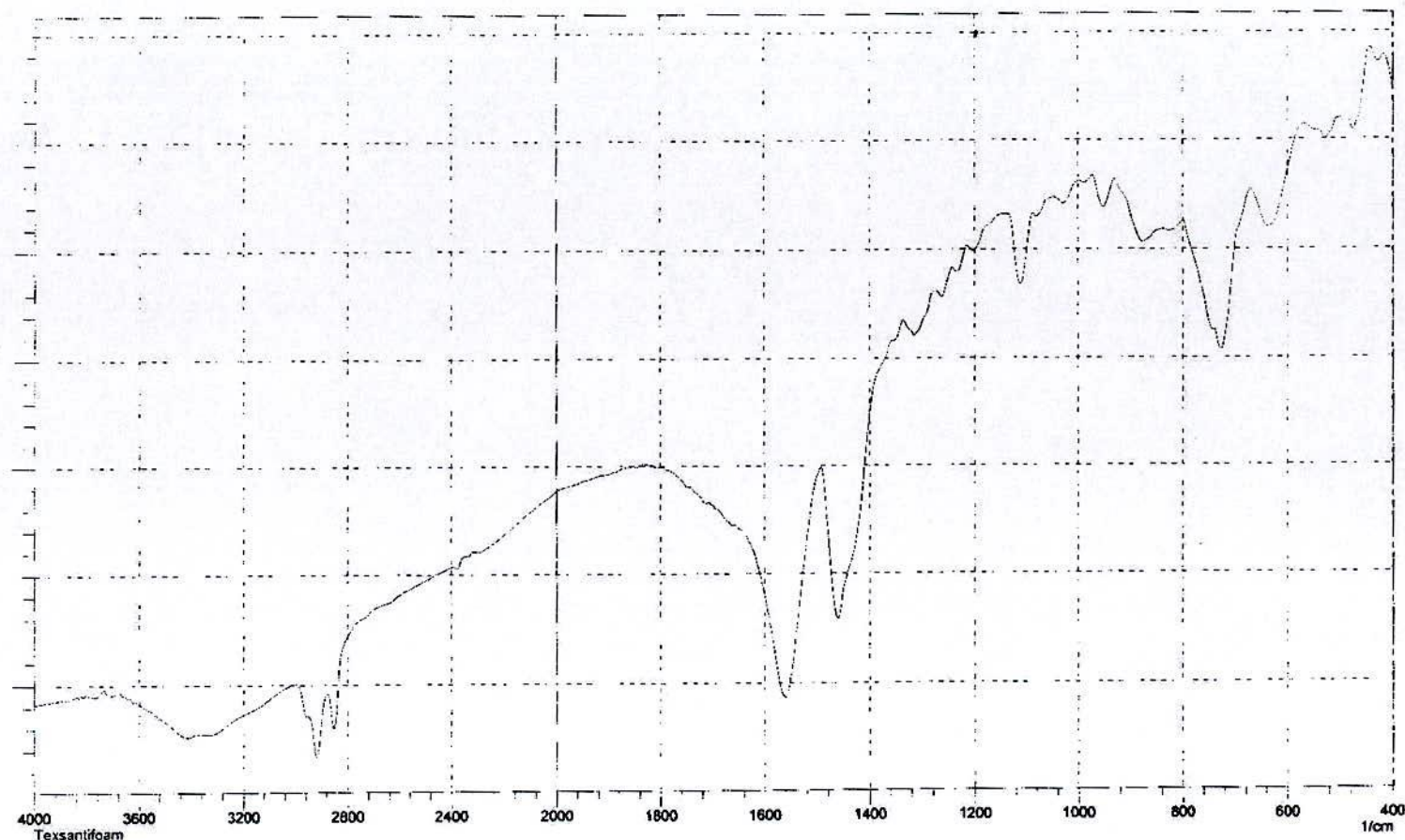


Figure 5.3: FTIR spectrum of Mg-laurate after heating at 90 °C

iment;
santifoam

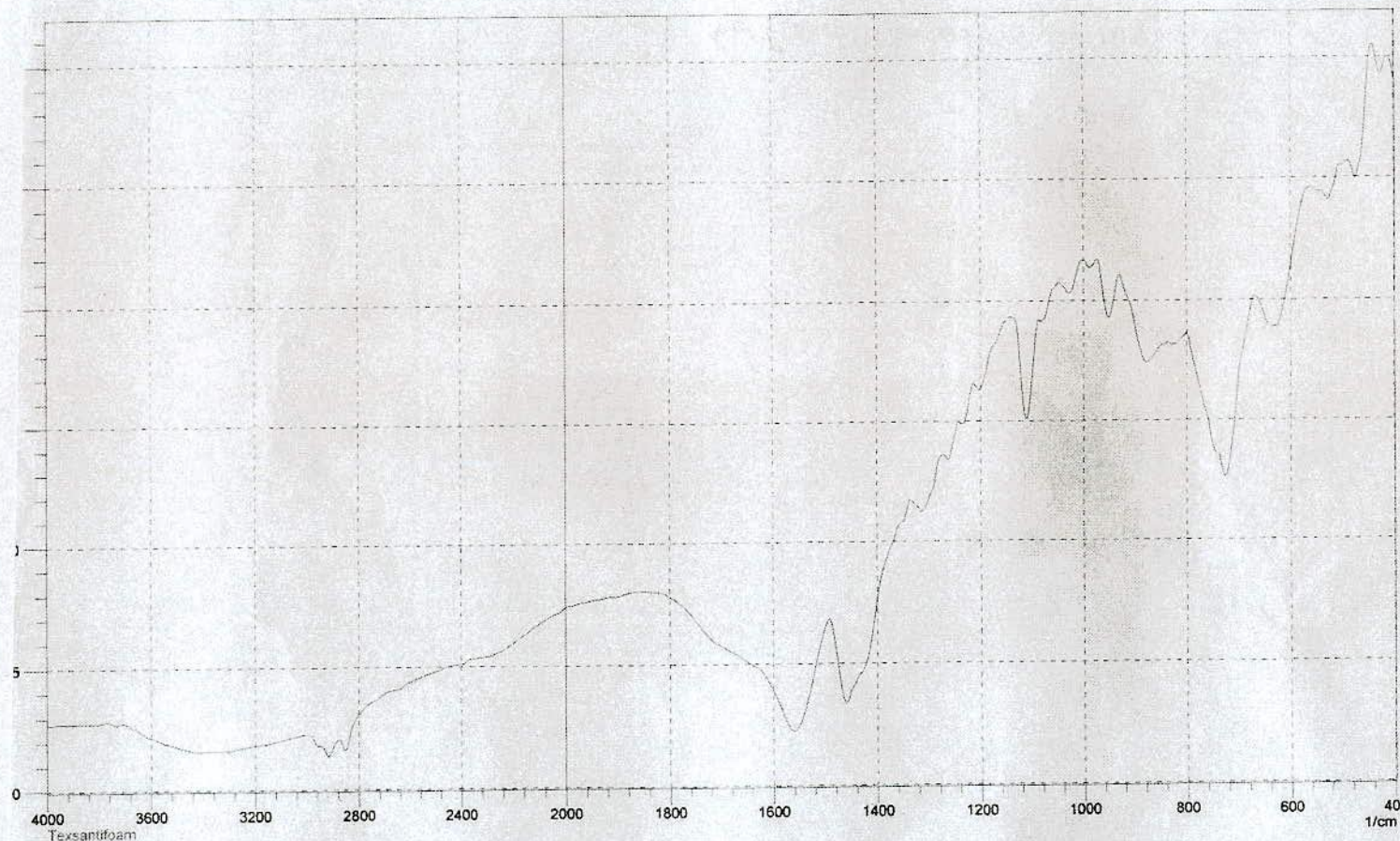
Apodization;
Resolution;

Date/Time; 4/19/2011 3:36:31 PM
User; Super

Table 5.3: Tentative assignment of IR bands of Mg-laurate after heating at 90 °C

Wave no. (cm^{-1})	Intensity %	Relative intensity	Tentative band assignment
3440	95	s, b	O-H stretching
2920	97	s, sh	Asymmetric C-H stretching
2865	95	s, sp	Symmetric C-H stretching
1560	91	s, sp	C=O stretching
1445	84	ms, sp	C-O stretching
1320	58	m, sp	-CH ₂ - bending
1120	53	m, sp	-CH ₃ bending

s = strong, ms = medium strong, m = medium, sp = sharp, b = broad, sh = shoulder



ment;
santifoam

Apodization;
Resolution;

Date/Time; 4/19/2011 3:49:40 PM
User; Super

Figure S.4: FTIR spectrum of Mg-laurate after heating at 110 °C

Table 5.4: Tentative assignment of IR bands of Mg-laurate after heating at 110 °C

Wave no. (cm^{-1})	Intensity %	Relative intensity	Tentative band assignment
3440	96	s, b	O-H stretching
2920	98	s, sh	Asymmetric C-H stretching
2860	96	s, sp	Symmetric C-H stretching
1565	94	s, b	C=O stretching
1445	92	ms, sh	C-O stretching
1320	77	m, sp	-CH ₂ - bending
1120	69	m, sp	-CH ₃ bending

s = strong, ms = medium strong, m = medium, sp = sharp, b = broad, sh = shoulder

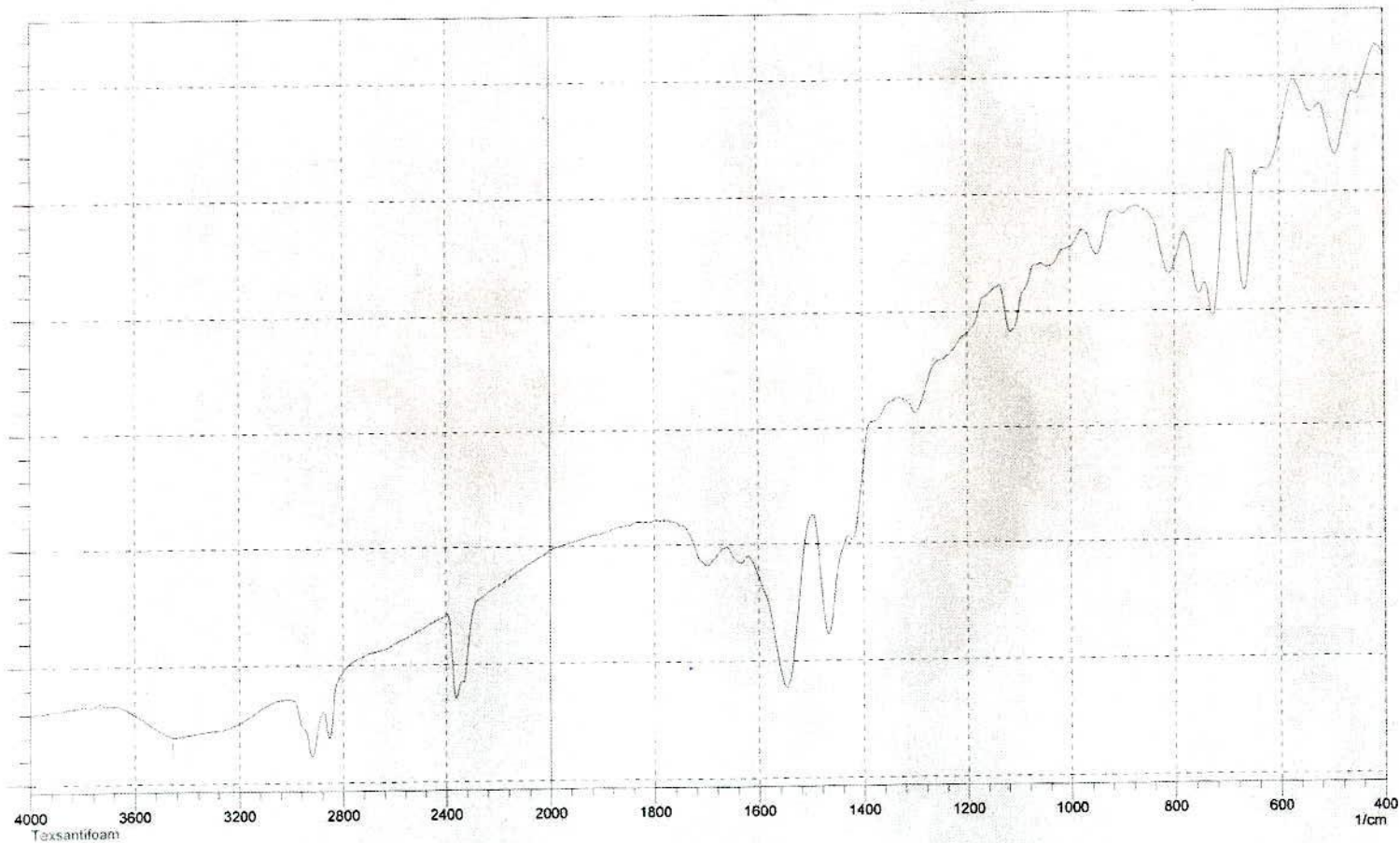


Figure 5.5: FTIR spectrum of Mg-myristate after heating at 90°C

ment;
santifoam

Apodization;
Resolution;

Date/Time; 4/19/2011 3:41:57 PM
User; Super

Table 5.5: Tentative assignment of IR bands of Mg-myristate after heating at 90 °C

Wave no. (cm^{-1})	Intensity %	Relative intensity	Tentative band assignment
3450	96	s, b	O-H stretching
2920	98	s, sh	Asymmetric C-H stretching
2850	97	s, sp	Symmetric C-H stretching
1555	91	s, b	C=O stretching
1445	88	ms, sh	C-O stretching
1325	68	m, sp	-CH ₂ - bending
1120	62	m, sp	-CH ₃ bending

s = strong, ms = medium strong, m = medium, sp = sharp, b = broad, sh = shoulder

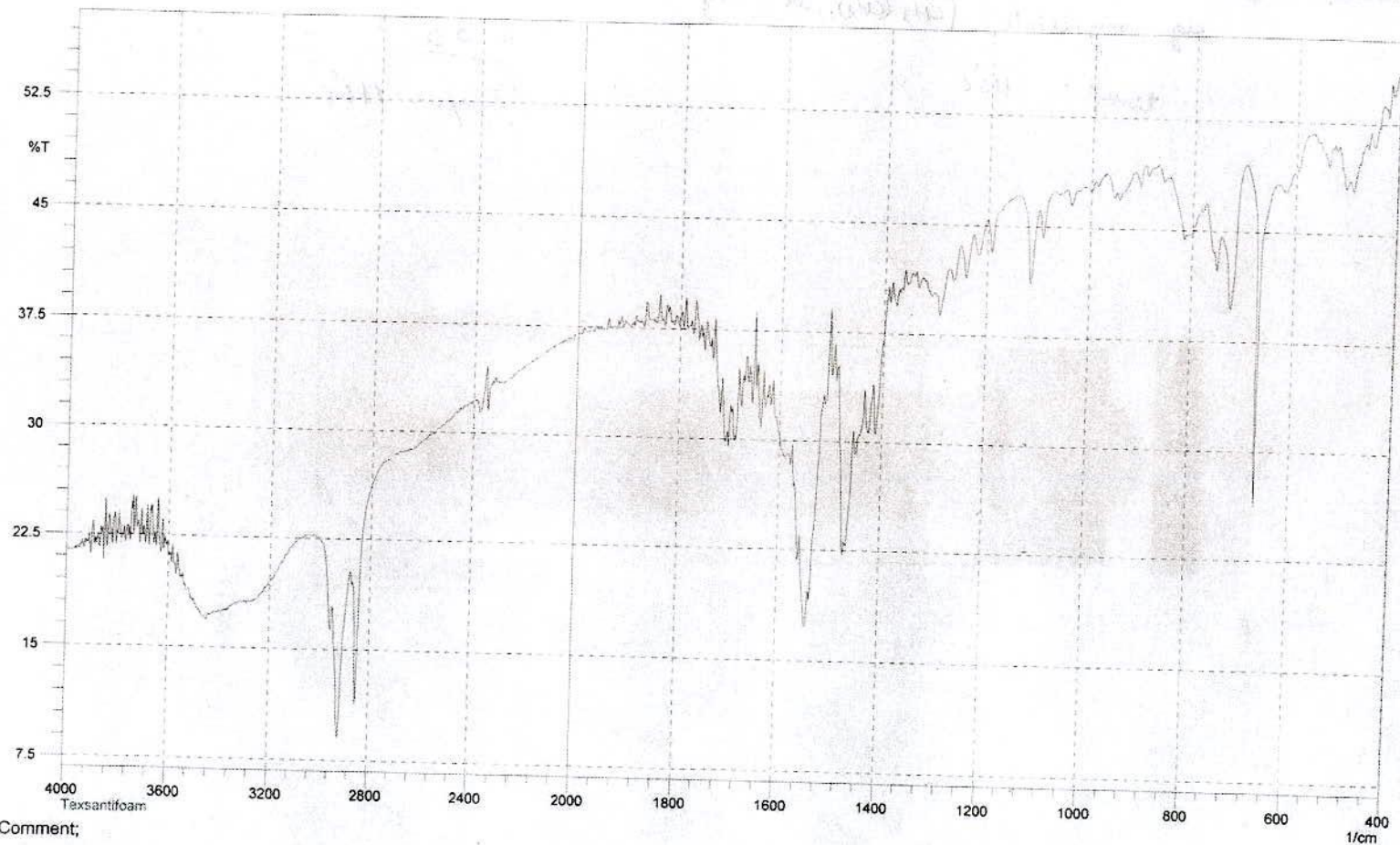


Figure 5.6: FTIR spectrum of Mg-myristate after heating at 110°C

Comment;
Teksantifoam

Apodization; Happ-Genzel
Resolution; 4 [1/cm]

Date/Time; 2/2/2011 4:14:10 PM
User; Super

Table 5.6: Tentative assignment of IR bands of Mg-myristate after heating at 110 °C

Wave no. (cm^{-1})	Intensity %	Relative intensity	Tentative band assignment
3450	87	ms, b	O-H stretching
2900	98	s, sh	Asymmetric C-H stretching
2840	95	s, sp	Symmetric C-H stretching
1540	86	s, b	C=O stretching
1470	80	ms, sh	C-O stretching
1295	68	m, sp	-CH ₂ - bending
1120	55	m, sp	-CH ₃ bending

s = strong, ms = medium strong, m = medium, sp = sharp, b = broad, sh = shoulder

Figure 5.7: FTIR spectrum of Mg-palmitate after heating at 90°C

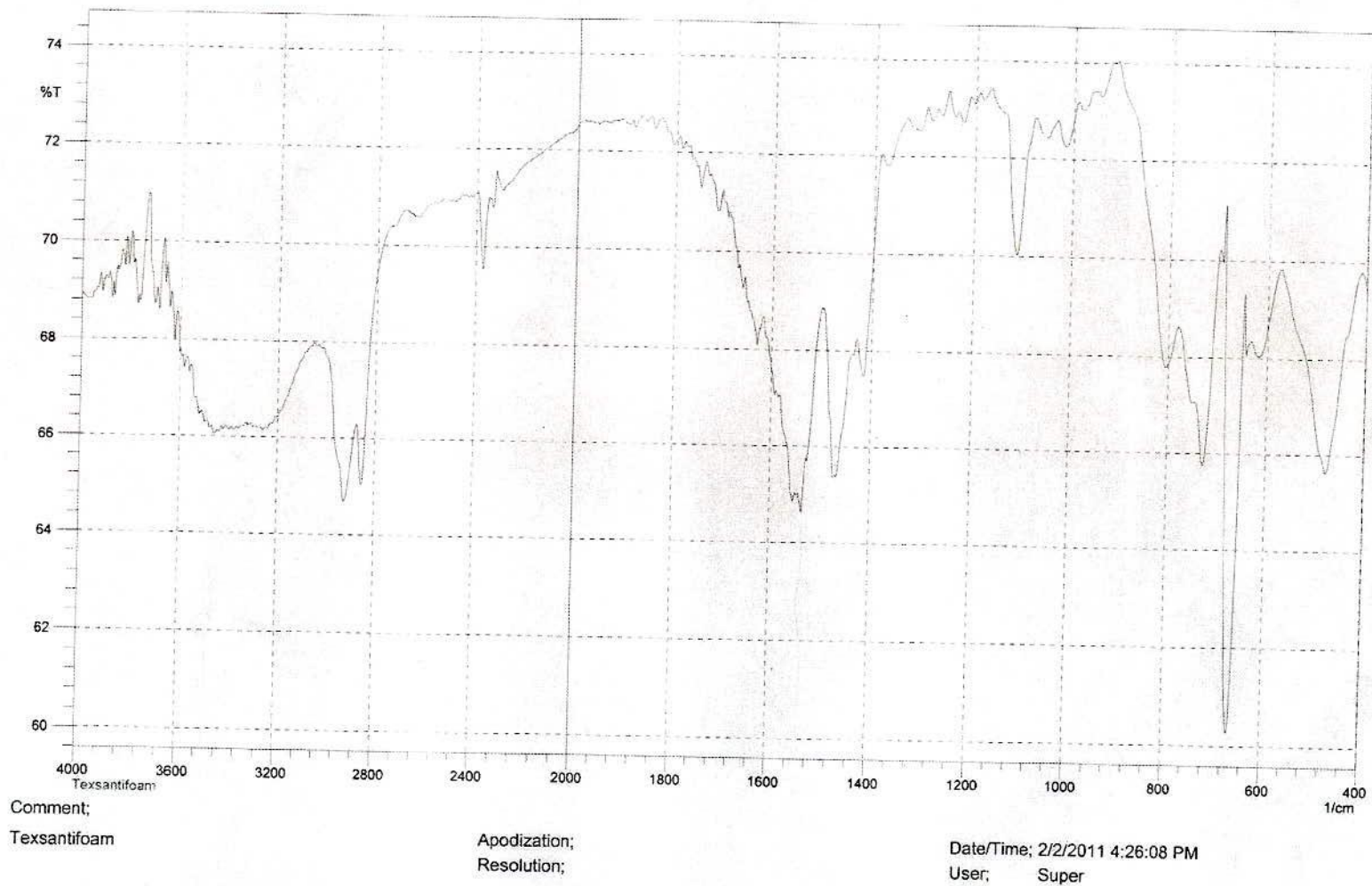
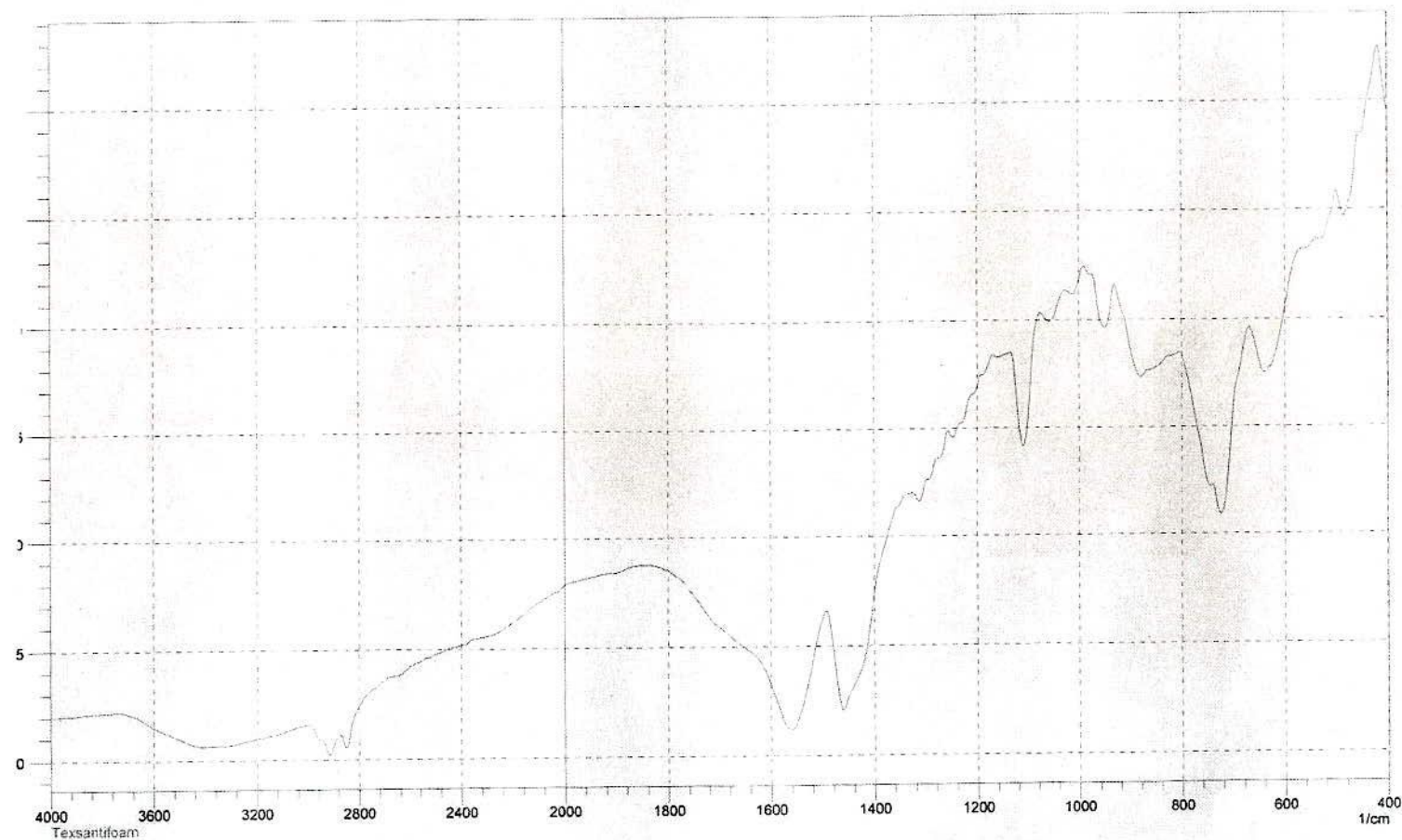


Table 5.7: Tentative assignment of IR bands of Mg-palmitate after heating at 90 °C

Wave no. (cm^{-1})	Intensity %	Relative intensity	Tentative band assignment
3480	69	m, b	O-H stretching
2900	77	ms, sh	Asymmetric C-H stretching
2850	75	ms, sp	Symmetric C-H stretching
1540	77	ms, b	C=O stretching
1480	72	ms, sh	C-O stretching
1320	48	m, b	-CH ₂ - bending
1110	50	m, sp	-CH ₃ bending

s = strong, ms = medium strong, m = medium, sp = sharp, b = broad, sh = shoulder



mmnt;
xsantifoam

Apodization;
Resolution;

Date/Time; 4/19/2011 3:44:38 PM
User; Super

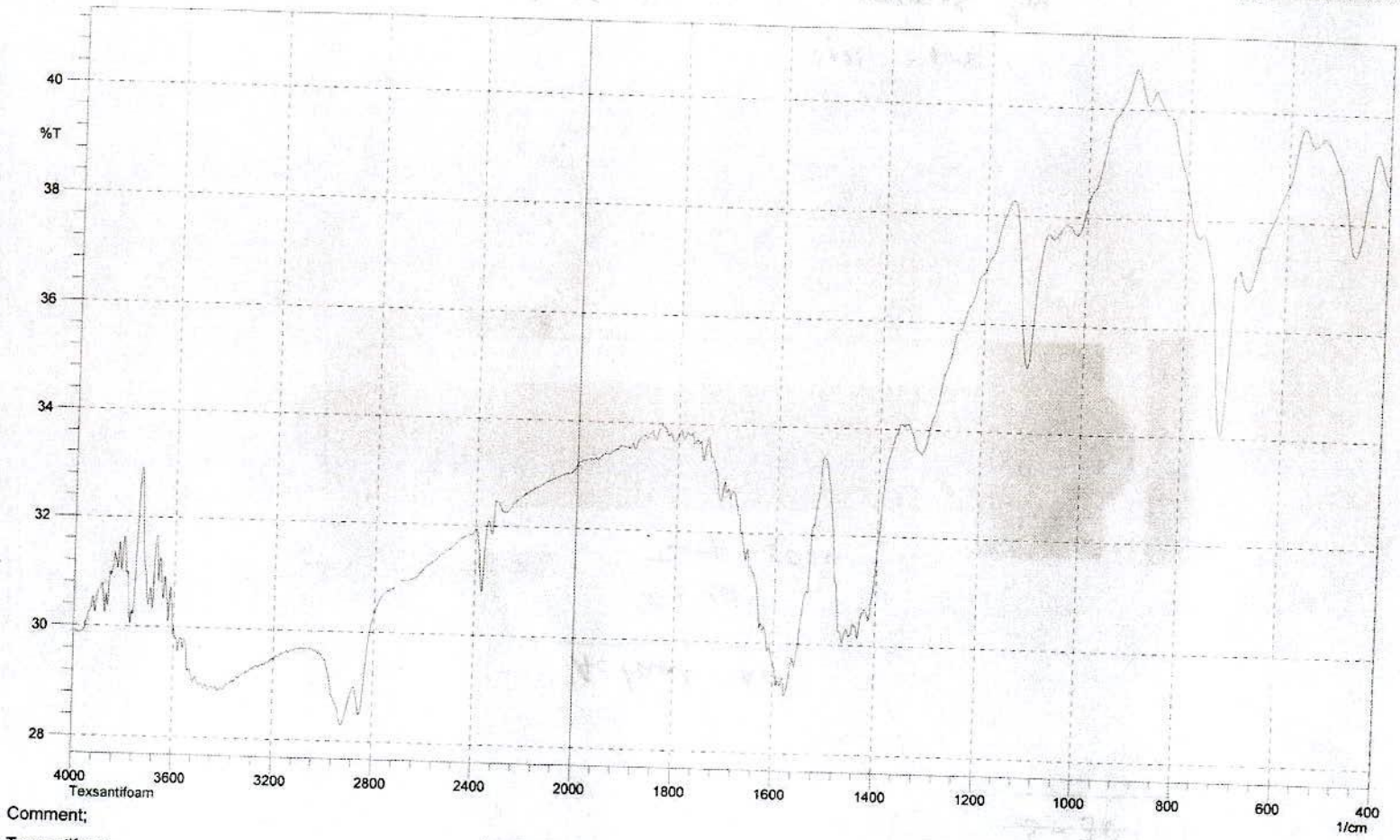
Figure 5.8: FTIR spectrum of Mg-palmitate after heating at 110°C

Table 5.8: Tentative assignment of IR bands of Mg-palmitate after heating at 110 °C

Wave no. (cm^{-1})	Intensity %	Relative intensity	Tentative band assignment
3480	97	s, b	O-H stretching
2900	99	s, sh	Asymmetric C-H stretching
2840	98	s, sp	Symmetric C-H stretching
1560	69	s, b	C=O stretching
1460	94	s, sh	C-O stretching
1320	76	ms, b	-CH ₂ - bending
1120	72	ms, sp	-CH ₃ bending

s = strong, ms = medium strong, m = medium, sp = sharp, b = broad, sh = shoulder

Figure 5.9: FTIR spectrum of Mg-stearate after heating at 90°C



Comment;
Texsantifoam

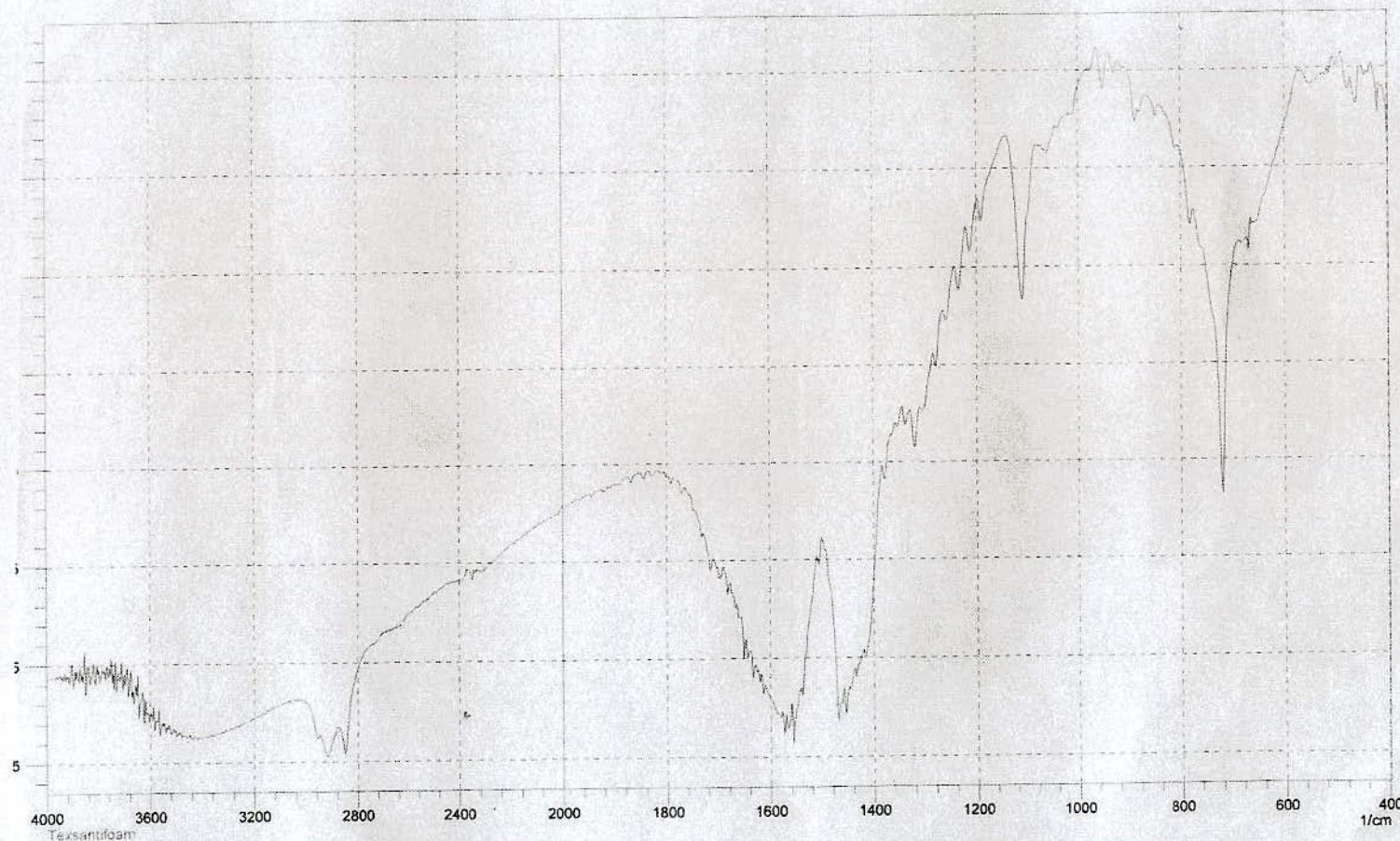
Apodization;
Resolution;

Date/Time; 2/2/2011 4:17:05 PM
User; Super

Table 5.9: Tentative assignment of IR bands of Mg-stearate after heating at 90 °C

Wave no. (cm^{-1})	Intensity %	Relative intensity	Tentative band assignment
3480	95	s, b	O-H stretching
2900	98	s, sh	Asymmetric C-H stretching
2840	97	s, sp	Symmetric C-H stretching
1570	94	s, b	C=O stretching
1460	89	ms, sh	C-O stretching
1320	72	ms, b	-CH ₂ - bending
1120	64	m, sp	-CH ₃ bending

s = strong, ms = medium strong, m = medium, sp = sharp, b = broad, sh = shoulder



ment;
:santifoam

Apodization; Happ-Genzel
Resolution; 4 [1/cm]

Date/Time; 4/19/2011 3:55:00 PM
User; Super

Figure 5.10: FTIR spectrum of Mg-stearate after heating at 110°C

Table 5.10: Tentative assignment of IR bands of Mg-stearate after heating at 110 °C

Wave no. (cm^{-1})	Intensity %	Relative intensity	Tentative band assignment
3480	97	s, b	O-H stretching
2900	99	s, sh	Asymmetric C-H stretching
2840	98	s, sp	Symmetric C-H stretching
1560	96	s, b	C=O stretching
1470	95	s, sh	C-O stretching
1320	68	ms, sp	-CH ₂ - bending
1120	52	m, sp	-CH ₃ bending

s = strong, ms = medium strong, m = medium, sp = sharp, b = broad, sh = shoulder

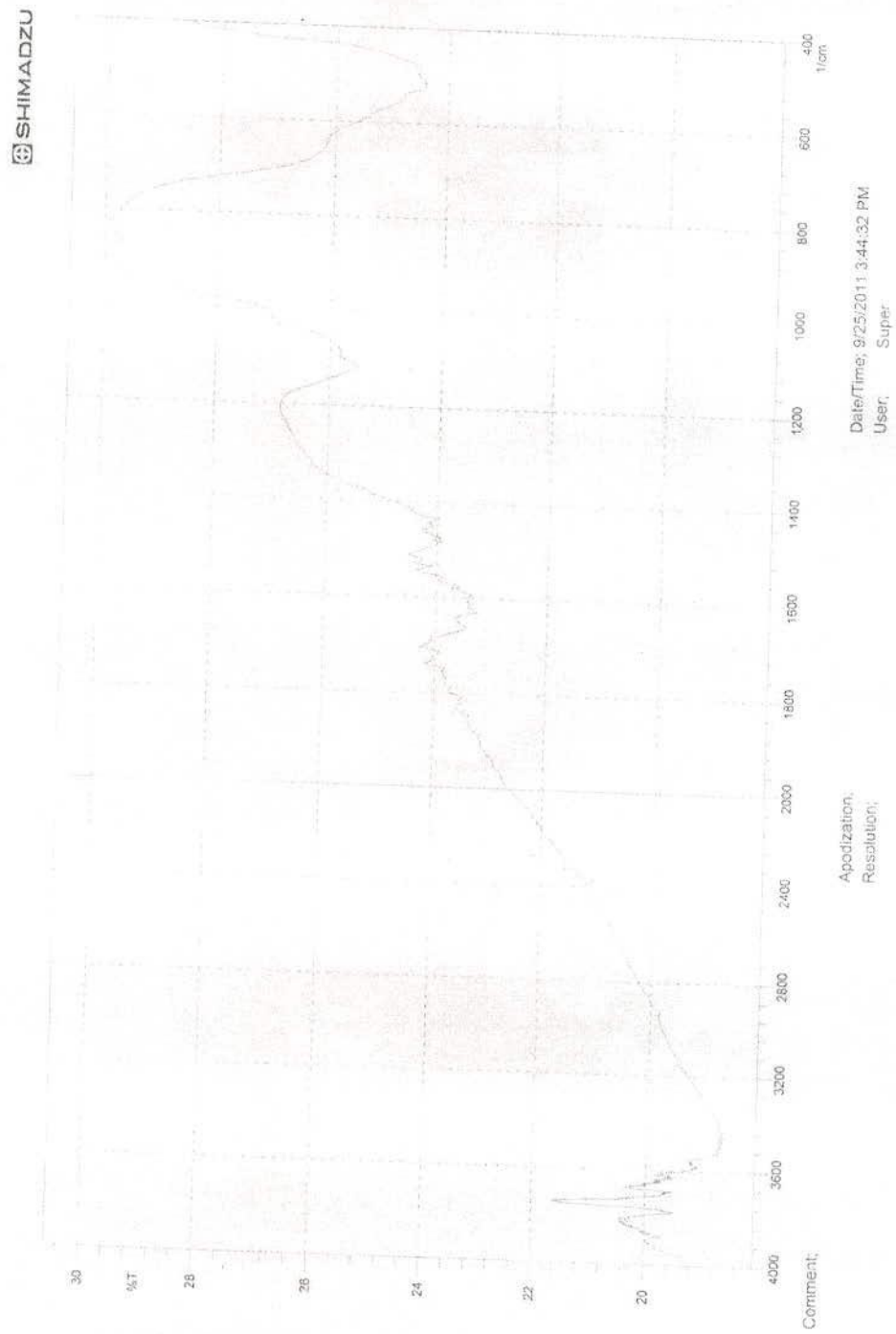


Figure 5.11: FTIR spectrum of Mg-NPs after heating at 600 °C for 4 hours

5.8 Transmission electron microscopy analyses

TEM was performed using a ZEISS EM10 transmission electron microscope operating at 80 kV. A diffraction grating replica was used to calibrate the images. NPs suspensions in toluene were drop cast onto 300-mesh copper grids and then were air-dried before viewing. Size and morphological analysis of the NPs was done manually on not less than 200 particles. The arrays of NPs are shown in figure 5.12. Figures 5.12(A), 5.12(B), 5.12(C) and 5.12(D) showed the TEM photograph of magnesium laurate, magnesium myristate, magnesium palmitate and magnesium stearate respectively. Scale bar represents 100 nm. It is seen that on an average, all the NPs are within 25-90 nm size range. At higher magnifications, these nanoparticles were recognized as spherical or oval in shape in all cases. Noteworthy variance was not found on the variation of chain length of the shell.

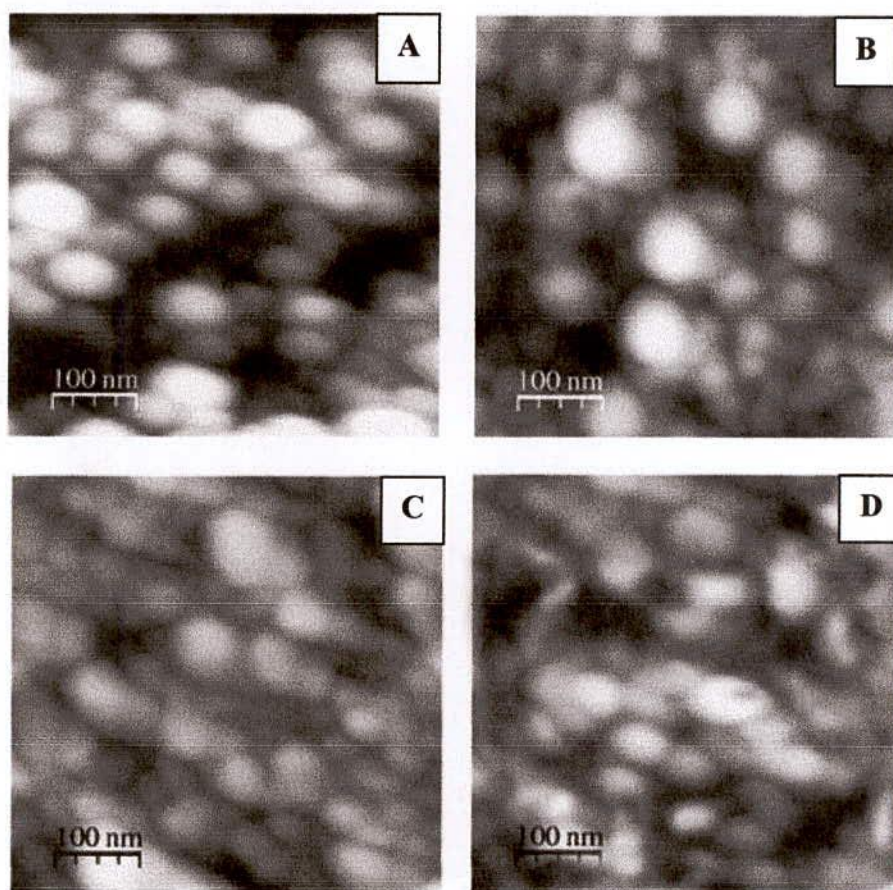


Figure 5.12: Transmission electron microscopy images of the prepared (A) magnesium laurate, (B) magnesium myristate, (C) magnesium palmitate and (D) magnesium stearate NPs.

5.9 Thermal Analysis

The thermo gravimetric analysis is a dynamic technique based on the change in the weight of a substance is recorded as the function of temperature or time. This technique is applied for the determination of the purity and thermal stability of both primary and secondary standards, the investigation of correct drying temperature and the suitability of various weighing forms for gravimetric analysis, and for the determination of the composition of Mg-NPs. It gives an idea about the bond strength of various constituent parts of the sample. Weight loss at lower temperature is generally due to removal of purely lattice component or other components. Such removal of components is generally endothermic. Generally, phase transition, dehydration reactions and some decomposition reactions provide endothermic effect, whereas crystalline, oxidation and some decomposition reactions produce exothermic effect. In the present study, the TGA of Mg-NPs were conducted in a temperature controlled Thermo Gravimetric Analyzer. The graphical presentations of these TG data and their characteristic features are recorded below.

The thermal analyses were obtained by TA Instruments-2100 thermal analysis system. Samples in the range of 16–30 mg but accurately weighed case to case were taken into an aluminum made crucible of which the volume was 100 μL . Then it was inserted in the furnace. The crucible was hermetically sealed, and a pinhole was punched into the crucible lid.

Magnesium laurate: The thermal behavior of the Mg-laurate has shown in figure 5.13. The broad nature of the TG trace indicated that the dehydration took place over a range of thermal events rather than a single temperature. 25.0 mg sample was taken in 100 μL Al crucible for analysis. About 9.8% weight loss was found between the temperature range of about 60–125 $^{\circ}\text{C}$. This may be due to the loss of moisture and crystalline water as reported earlier [87] and also supports the moisture content as mentioned in section 5.5. Essential weight losses revealed by TG are in good agreement of DTA results as can be described by the endotherm at about 105 $^{\circ}\text{C}$. The exotherm at around 145 $^{\circ}\text{C}$ may be corresponded to melting. The exotherm at 265 $^{\circ}\text{C}$ may be assigned to the combustion of hydrocarbon part of the shell of NPs. At the temperature above 340 $^{\circ}\text{C}$ more than 80.0% weight has been lost. This may be

due to the loss of organic part of NPs as confirmed by the corresponding exotherm obtained from DTA. The loss of organic parts at higher temperatures also corresponds to the decomposition of the NPs at higher temperature in a normal furnace as investigated by FTIR shown in figure 5.11. The weight losses by thermal analyses have been tabulated in table 5.11.

Table 5.11: Weight loss recorded at different stages of TGA of Mg-laurate NPs

Mg-laurate NPs	TG analysis		Probable Findings
	Transition temp. (°C)	% Wt. loss	
Mg(C ₁₂ H ₂₃ O ₂) ₂	60-125	9.8	The weight loss may be due to loss of moisture and crystalline water
	>350	80	The weight loss may be due to loss of organic part

Magnesium myristate: The thermal behavior of the Mg-myristate has shown in figure 5.14. The broad nature of the TG trace indicated that the dehydration took place over a range of thermal events rather than a single temperature. 20.0 mg sample was taken in 100 μ L Al crucible for analysis. About 30% weight loss was found between the temperature range of about 60–140 °C. It is speculated that the sample was damp or moist. This may be due to the loss of a lot of moisture or adhering water molecules and crystalline water as reported earlier [87] although this results do not come to an agreement of the moisture content as mentioned in section 5.5. The exotherm at about 130 °C may be corresponded to melting. Essential weight losses revealed by TG are in good agreement of DTA results as can be described by a very weak endotherm at 65 °C and a sharp, intense endotherm at about 115 °C. The exotherm at 220 °C may be assigned to the combustion of hydrocarbon part of the shell of NPs. At the temperature range of 350–450 °C about 60% weight has been lost. This may be due to the loss of organic part of NPs as confirmed by the corresponding exotherm obtained from DTA. The loss of organic parts at higher temperatures also corresponds to the decomposition of the NPs at higher temperature in a normal furnace as investigated by FTIR shown in figure 5.11. The results of thermal analyses have been tabulated in table 5.12.

Table 5.12: Weight loss recorded at different stages of TGA of Mg-myristate NPs

Mg-myristate NPs	TG analysis		Probable Findings
	Transition temp. (°C)	% Wt. loss	
Mg(C ₁₄ H ₂₇ O ₂) ₂	60-140	30	The sample was damp or moist. The weight loss may be due to loss of adhering water, moisture and crystalline water
	350-450	60	The weight loss may be due to loss of organic part

Magnesium palmitate: The thermal behavior of the Mg-palmitate has shown in figure 5.15. The broad nature of the TG trace indicated that the dehydration took place over a range of thermal events rather than a single temperature. 16.0 mg sample was taken in 100 μ L Al crucible for analysis. About 11.25% weight loss was found between the temperature range of about 60–140 °C. This may be due to the loss of a lot of moisture and crystalline water as reported earlier [87] and also relates the moisture content as cited in section 5.5. Essential weight losses revealed by TG are in good agreement of DTA results as can be described by the endotherm at 80 °C and a sharp, intense endotherm at about 115 °C. The exotherm at 260 °C may be assigned to the combustion of hydrocarbon part of the shell of NPs. At the temperature range of 320–440 °C about 81.1% weight has been lost. This may be due to the loss of organic part of NPs as confirmed by the corresponding exotherm obtained from DTA. The loss of organic parts at higher temperatures also corresponds to the decomposition of the NPs at higher temperature in a normal furnace as investigated by FTIR shown in figure 5.11. The results of thermal analyses have been tabulated in table 5.13.

Table 5.13: Weight loss recorded at different stages of TGA of Mg- palmitate NPs

Mg-palmitate NPs	TG analysis		Probable Findings
	Transition temp. (°C)	% Wt. loss	
Mg(C ₁₆ H ₃₁ O ₂) ₂	60-140	11.25	The weight loss may be due to loss of moisture and crystalline water
	320-440	81.1	The weight loss may be due to loss of organic part

Magnesium stearate: The thermal behavior of the Mg-stearate has shown in figure 5.16. The broad nature of the TG trace indicated that the dehydration took place over a range of thermal events rather than a single temperature. 30.0 mg sample was taken in 100 μ L Al crucible for analysis. About 11.6% weight loss was found between the temperature range of about 65–140 °C. This may be due to the loss of a lot of moisture and crystalline water as reported earlier [87] and also relays the moisture content as stated in section 5.5. Essential weight losses revealed by TG are in good agreement of DTA results as can be described by the endotherm at 90 °C and a sharp, intense endotherm at about 120 °C. The exotherm at 170 °C may be assigned to the combustion of hydrocarbon part of the shell of NPs. At the temperature range of 325–440 °C about 73.5% weight has been lost. This may be due to the loss of organic part of NPs as confirmed by the corresponding exotherm obtained from DTA. The loss of organic parts at higher temperatures also corresponds to the decomposition of the NPs at higher temperature in a normal furnace as investigated by FTIR shown in figure 5.11. The results of thermal analyses have been tabulated in table 5.14.

Table 5.14: Weight loss recorded at different stages of TGA of Mg- stearate NPs

Mg-palmitate NPs	TG analysis		Probable Findings
	Transition temp. (°C)	% Wt. loss	
Mg(C ₁₈ H ₃₅ O ₂) ₂	65-140	11.6	The weight loss may be due to loss of moisture and crystalline water
	350–440	73.5	The weight loss may be due to loss of organic part

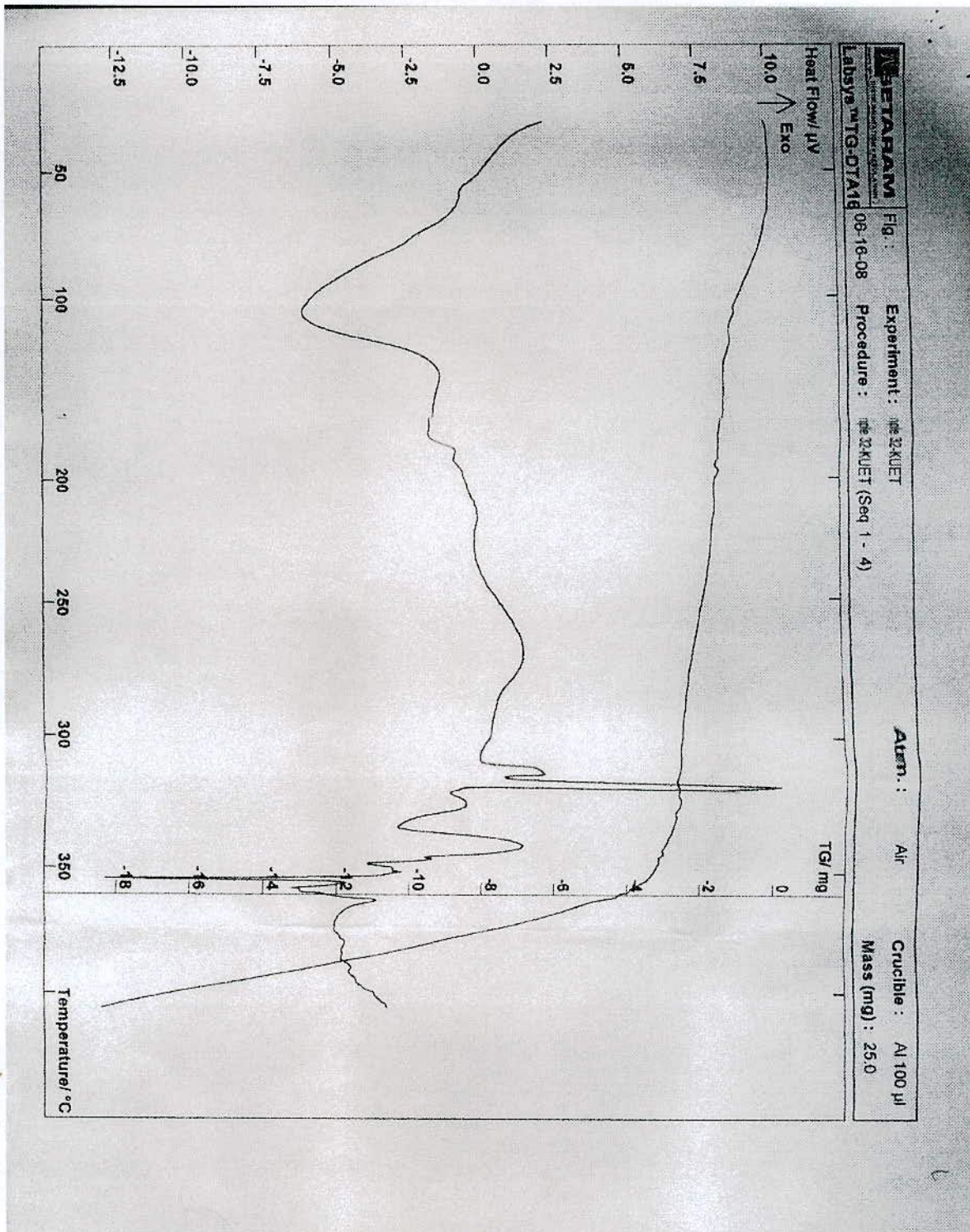


Figure 5.13: Thermal Analysis of Mg-laurate NPs

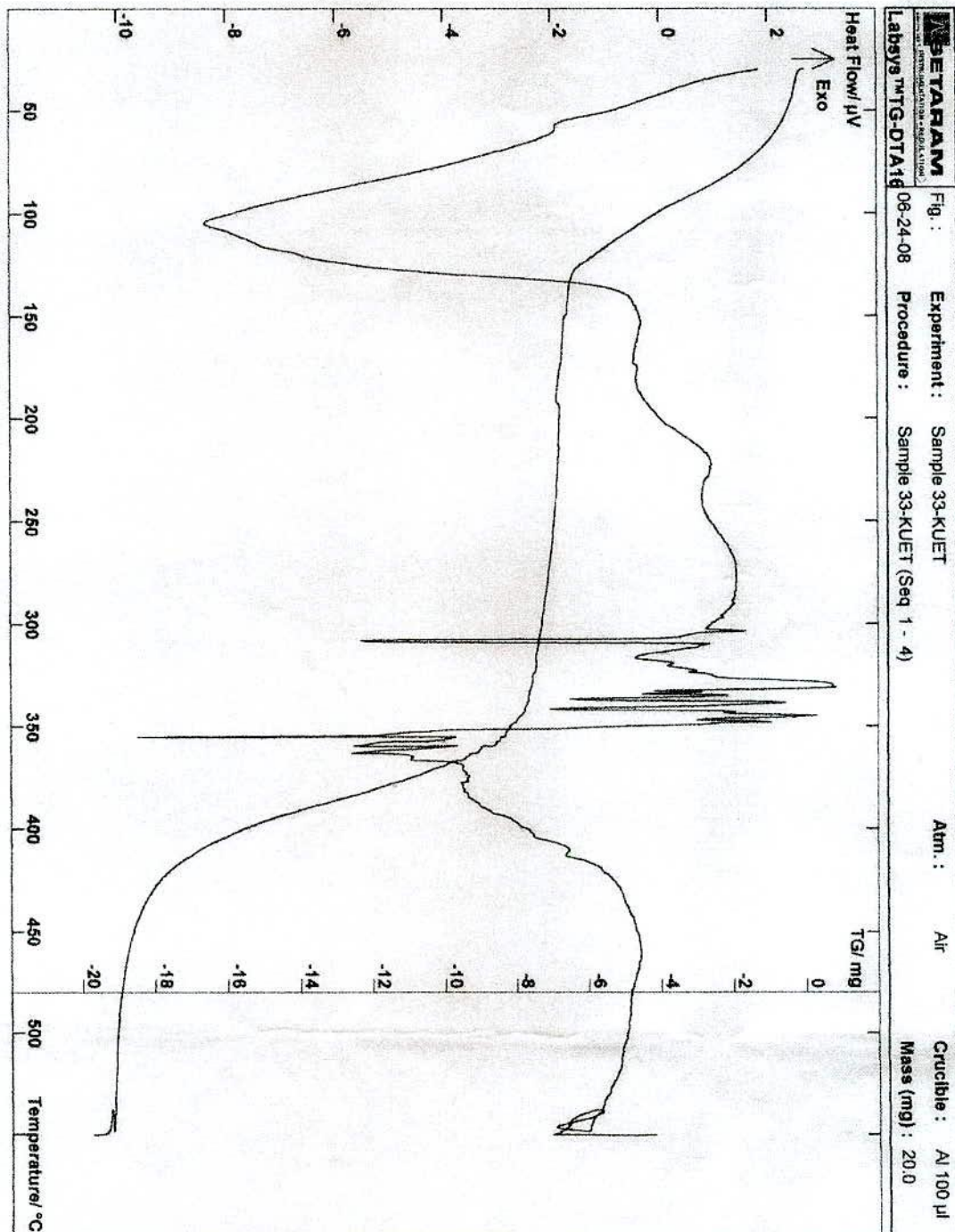


Figure 5.14: Thermal Analysis of Mg-myristate NPs

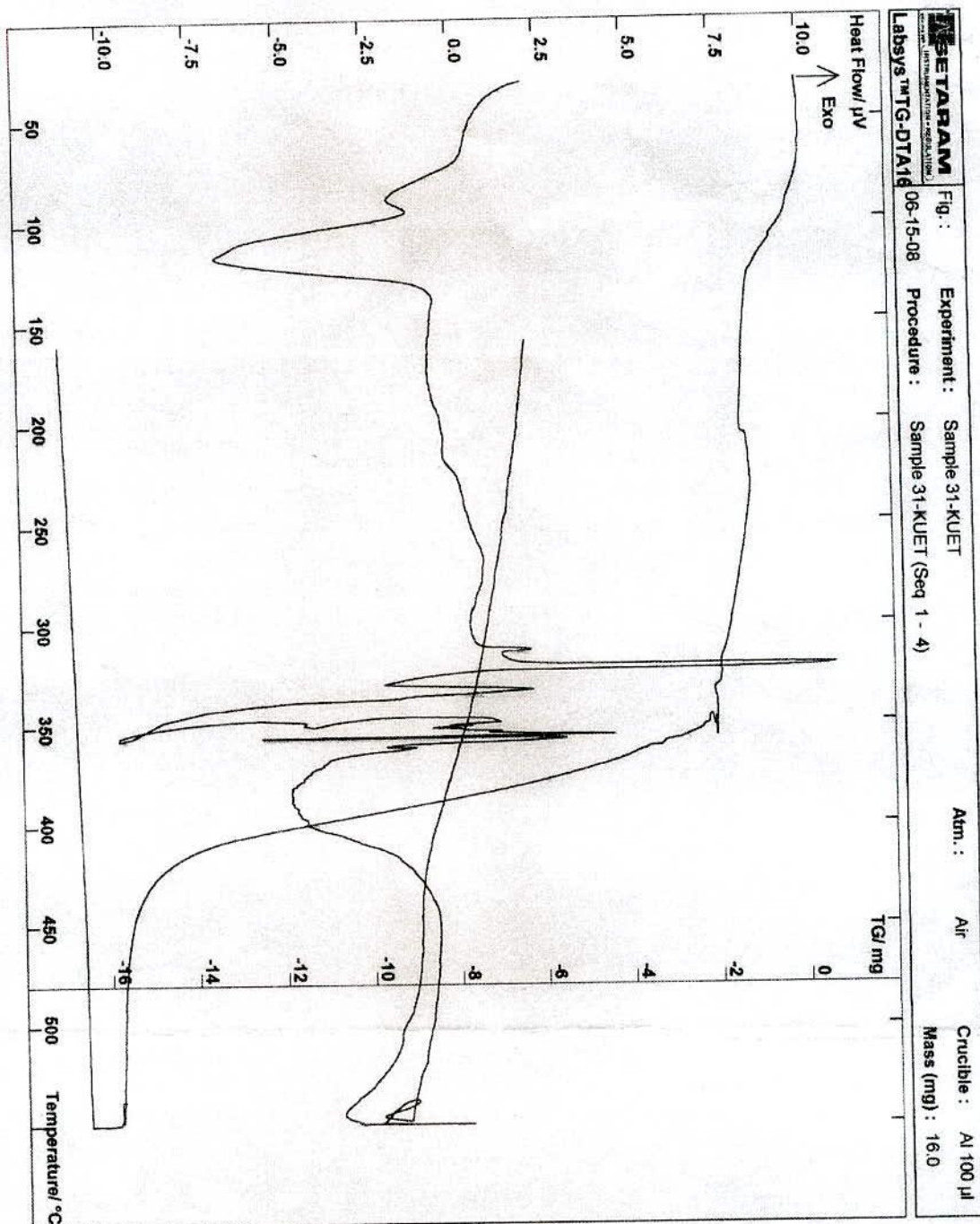


Figure 5.15: Thermal Analysis of Mg-palmitate NPs

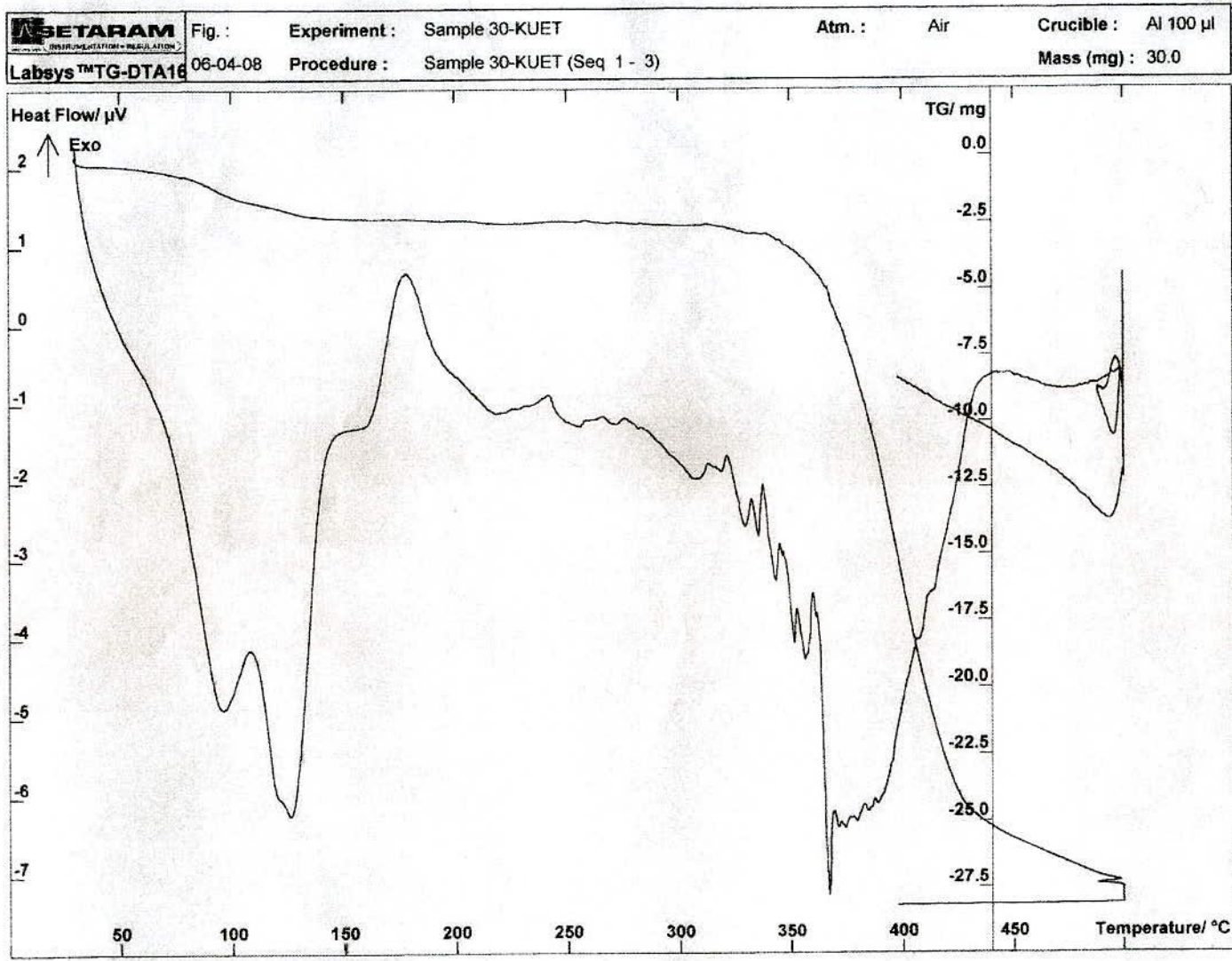


Figure 5.16: Thermal Analysis of Mg-stearate NPs

CHAPTER VI

Conclusion

Long chain alkyl carboxylate shell protected magnesium; core-shell nanoparticles have been synthesized. The syntheses procedures involve two steps. The shells are long chain alkyl carboxylates and the core is magnesium metal. Elemental analysis, optical and spectral studies showed the crucial evidence in favor of core-shell nanoparticles. TEM analysis showed that the particles have the dimensions in the range of 25–90 nm in size. Thermal analyses of the NPs suggest that there is moisture and/or crystalline water and the alkyl carboxylates or organic part in the samples.

References

- 1 Wiley, B., Sun, Y., Chen, J., Cang, H., Li, Z.Y., Li, X., Xia, Y., 2008, "Shape-controlled synthesis of silver and gold nanostructures," *MRS Bulletin*, Vol. 30, pp. 356-361.
- 2 Tsutsui, G., Huang, S., Sakaue, H., Shingubara, S., Takahagi, T., 2001, "Well-size-controlled colloidal gold nanoparticles dispersed in organic solvents," *Japanese Journal of Applied Physics, Part 1: Regular Papers, Short Notes & Review Papers*, Vol. 40, pp. 346-349.
- 3 Lu, X., Hsing, Y.T., Brian, A.K., Xia, Y., 2008, "Facile synthesis of gold nanoparticles with narrow size distribution by using AuCl or AuBr as the precursor," *Chemistry--A European Journal*, Vol. 14, pp. 1584-1591.
- 4 Mandal, S., Selvakannan, P.R., Pasricha, S.P.R., Sastry, M., 2002, "Synthesis of a stable gold hydrosol by the reduction of chloroaurate ions by the amino acid, aspartic acid," *Proceedings - Indian Academy of Sciences, Chemical Sciences*, Vol. 114, pp. 513-520.
- 5 Lee, T.M.-H., Li, L.-L., Hsing, I.-M., 2003, *Langmuir*, Vol. 19, pp. 4338.
- 6 Poizot, P., Laruelle, S., Grugeon, S., Dupont, L., Tarascon, J.M., 2000, *Nature*, Vol. 407, pp. 496.
- 7 Ross, C., 2001, *Annu. Rev. Mater. Res.*, Vol. 31, pp. 203.
- 8 Colvin, V.L., Schlamp, M.C., Alivisatos, A.D., 1994, *Nature*, Vol. 370, pp. 354.
- 9 Alexey, R., Novick, R.P., 2000, "Equivalence of Lauric Acid and Glycerol Monolaurate as Inhibitors of Signal Transduction in *Staphylococcus aureus*". *J Bacteriol*, Vol. 182 (9), pp. 2668-2671.

- 10 Emsley, J., 2001, "Nature's Building Blocks: An A-Z Guide to the Elements", Oxford:Oxford University Press, pp. 43, 513, 529.
- 11 Beare-Rogers J., Dieffenbacher A., Holm J. V., 2001, "Lexicon of lipid nutrition (IUPAC Technical Report)", Pure and Applied Chemistry, Vol. 73 (4), pp. 685–744.
- 12 Beare-Rogers, J., Dieffenbacher, A., Holm, J.V., 2001, "Lexicon of lipid nutrition (IUPAC Technical Report)", Pure and Applied Chemistry, Vol. 73 (4), pp. 685–744.
- 13 Sootthikanokkhan, J., Tunjongnawin, P., 2002, "Investigation of the effect of mixing schemes on cross-link distribution and tensile properties of natural–acrylic rubber blends", Polymer Testing, Vol. 22 (3), pp. 305–312.
- 14 Tsenga, W.J., Mo, L.D., Hsub, C.K., 1999, "Influence of stearic acid on suspension structure and green microstructure of injection-molded zirconia ceramics", Ceramics International, Vol. 25 (2), pp. 191–195.
- 15 Hunter, J.E., Zhang, J., Kris-Etherton, P.M., 2010, "Cardiovascular disease risk of dietary stearic acid compared with trans, other saturated, and unsaturated fatty acids: a systematic review", Am. J. Clinical Nutrition (American Society for Nutrition), Vol. 91(1), pp. 46–63.
- 16 Søndergaard, D., Meyera O., Würtzena, G., 1980, "Magnesium stearate given peroperally to rats. A short term study", Toxicology, Vol. 17 (1), pp. 51–55.
- 17 Ritter, S., 2008, "What's That Stuff? Excipients: Inactive ingredients in medicines serve multiple functions in drug delivery", Chemical & Engineering News, Vol. 86 (1), pp. 025.
- 18 Sworbrick, J., James, C.B., 1990, Encyclopedia of pharmaceutical technology, pp. 2274.
- 19 Weiner, M.L., Lois, A. K., 1999, Excipient Toxicity and Safety, pp. 10.

- 20 Uzunović, A., Vranić, E., 2007, "Effect of Magnesium Stearate Concentration On Dissolution Properties Of Ranitidine Hydrochloride Coated Tablets", *Bosnian Journal Of Basic Medical Sciences*, Vol. 7(3), pp. 279-283.
- 21 Xia, C., Advincula, R.C., 2001, *Chem. Mater*, Vol. 13, pp. 1674.
- 22 Yin, B., Ma, H., Wang, S., Chen, S., 2003, *J. Phys. Chem. B*, Vol. 107, pp. 8898.
- 23 Rodr'iguez-S'anchez, L., Blanco, M.C., L'opez-Quintela, M.A., 2000, *J. Phys. Chem. B*, Vol. 104, pp. 9683.
- 24 Raveendran, P., Fu, J., Wallen, S.L., 2003, *J. Am. Chem. Soc.*, Vol. 125, pp. 13940.
- 25 Mukherjee, P., Ahmad, A., Mandal, D., Senapati, S., Sainkar, S.R., Khan, M.I., Parishcha, R., Ajaykumar, P.V., Alam, M., Kumar, R., Sastry, M., 2001, *Nano. Lett.* Vol. 1 pp. 515.
- 26 Gardea-Torresdey, J.L., Gomez, E., Peralta-Videa, J.R., Parsons, J.G., Troiani, H., Jose-Yacaman, M., 2003, *Langmuir*, Vol. 19, pp. 1357.
- 27 Hayashi, T., Ohno, T., Yatsuya, S., Uyeda, R., 1977, *J. Appl. Phys.*, Vol. 16, pp. 705.
- 28 Mafune, F., Kohno, J., Takeda, Y., Kondow, T., 2000, *J. Phys. Chem. B*, Vol. 104, pp. 8333.
- 29 Brugger, P.A., Guendet, P., Gratzel, M., 1981, *J. Am. Chem. Soc.*, Vol. 103, pp. 2923.
- 30 Shibata, S., Aoki, K., Yano, T., Yamane, M.J., 1998, *Sol-Gel Sci. Technol.*, Vol. 11, pp. 279.
- 31 Pol, V.G., Srivastava, D.N., Palchik, O., Palchik, V., Slifkin, M.A., Weiss, A.M., Gedanken, A., 2002, *Langmuir*, Vol. 18, pp. 3352.
- 32 Wang, T.C., Rubner, M.F., Cohen, R.E., 2002, *Langmuir*, Vol. 18, pp. 3370.

- 33 Sun, S., Anders, S., Hamann, H.F., Thiele, J.-U., Baglin, J.E.E., Thomson, T., Fullerton, E.E., Murray, C.B., Terris, B.D., 2002, *J. Am. Chem. Soc.* Vol. 124, pp. 2884.
- 34 Dai, J., Bruening, M.L., 2002, *Nano Lett.* Vol. 2, pp. 497.
- 35 Manna, A., Imae, T., Iida, M., Hisamatsu, N., 2001, *Langmuir*, Vol. 17, pp. 6000.
- 36 Lin, X.Z., Teng, X., Yang, H., 2003, *Langmuir*, Vol. 19, pp. 10081.
- 37 Nagasawa, H., Maruyama, M., Komatsu, T., Isoda, S., Kobayashi, T., 2002, *Phys. Stat. Sol. (a)*, Vol. 191, pp. 67.
- 38 Kuwajima, S., Okada, Y., Yoshida, Y., Abe, K., Tanigaki, N., Yamaguchi, T., Nagasawa, H., Sakurai, K., Yase, K., 2002, *Colloid Surf. A*, Vol. 197, pp. 1.
- 39 Abe, K., Hanada, T., Yamaguchi, T., Takiguchi, H., Nagasawa, H., Nakamoto, M., Yase, K., 1998, *Mol. Cryst. Liq. Cryst.*, Vol. 322, pp. 173.
- 40 Cheng, W., Dong, S., Wang, E., 2002, *Electrochem. Commun.*, Vol. 4, pp. 412.
- 41 Johans, C., Clohessy, J., Fantini, S., Kontturi, K., Cunnane, V.J., 2002, *Electrochem. Commun.*, Vol. 4, pp. 227.
- 42 Aslam, M., Chaki, N.K., Mulla, I.S., Vijayamohan, K., *Appl. Surf. Sci.*, Vol. 182, pp. 338.
- 43 Stiger, R.M., Gorer, S., Craft, B., Penner, R.M., 1999, *Langmuir*, Vol. 15, pp. 790.
- 44 Sibbald, M.S., Chumanov, G., Cotton, T.M., 1997, *J. Electroanal. Chem.*, Vol. 438, pp. 179.
- 45 Bright, R.M., Musick, M.D., Natan, M.J., 1998, *Langmuir*, Vol. 14, pp. 5695.
- 46 Lee, P.C., Meisel, D., 1982, *J. Phys. Chem.*, Vol. 86, pp. 3391.

- 47 Lee, N.-S., Sheng, R.-S., Morris, M.D., Schopfer, L.M., 1986, *J. Am. Chem. Soc.*, Vol. 108, pp. 6179.
- 48 Aoki, K., Chen, J., Yang, N., Nagasawa, H., *Langmuir*, 2003, Vol. 19, pp. 9904.
- 49 Yang, N., Aoki, K., Nagasawa, H., 2004, *J. Phys. Chem. B*, Vol. 108, pp. 15027.
- 50 Xiaohui, J., Xiangning, S., Li, J., Bai, Y., Yang, W., Peng, X., 2007, "Size Control of Gold Nanocrystals in Citrate Reduction: The Third Role of Citrate," *J. Am. Chem. Soc.*, Vol. 129, pp. 13939-13948.
- 51 Kumar, S., Gandhi, K.S., Kumar, R., 2007, "Modeling of formation of gold nanoparticles by citrate method," *Industrial & Engineering Chemistry Research*, Vol. 46, pp. 3128-3136.
- 52 Chiang, C.L., Hsu, M.B., Lai, L.B., 2004. "Control of nucleation and growth of gold nanoparticles in AOT/Span80/isooctane mixed reverse micelles," *Journal of Solid State Chemistry*, Vol. 177, pp. 3891-3895.
- 53 Srisombat, L.O., Park, J.S., Zhang, S. Lee, T.R., 2008, "Preparation, Characterization, and Chemical Stability of Gold Nanoparticles Coated with Mono-, Bis-, and Tris-Chelating Alkanethiols," *Langmuir*, Vol. 24, pp. 7750-7754.
- 54 Zhang, F., Skoda, M.W.A., Jacobs, R.M.J., Zorn, S., Martin, R.A., Martin, C.M., Clark, G.F., Goerigk, G., Schreiber, F., 2007, "Gold nanoparticles decorated with oligo(ethylene glycol) thiols: protein resistance and colloidal stability," *Journal of Physical Chemistry A*, Vol. 111, pp. 12229-12237.
- 55 Matsuura, K., Ohno, K., Kagaya, S., Kitano, H., 2007, "Carboxybetaine polymer-protected gold nanoparticles: high dispersion stability and resistance against non-specific adsorption of proteins," *Macromolecular Chemistry and Physics*, Vol. 208, pp. 862-873.
- 56 Miyamoto, D., Oishi, M., Kojima, K., Yoshimoto, K., Nagasaki, Y., 2008, "Completely Dispersible PEGylated Gold Nanoparticles under Physiological Conditions:

- Modification of Gold Nanoparticles with Precisely Controlled PEG-bpolyamine," *Langmuir*, Vol. 24, pp. 5010-5017.
- 57 Otsuka, H., Nagasaki, Y., Kataoka, K., 2003, "PEGylated nanoparticles for biological and pharmaceutical applications," *Advanced Drug Delivery Reviews*, Vol. 55, pp. 403-419.
- 58 Keitaro Yoshimoto, K., Yuki Hoshino, Y., Takehiko Ishii, T., and Yukio Nagasaki, Y., 2008, "Binding enhancement of antigen-functionalized PEGylated gold nanoparticles onto antibody-immobilized surface by increasing the functionalized antigen using *α*-sulfanyl- ω -amino-PEG," *Chemical Communications (Cambridge, United Kingdom)*, pp. 5369-5371.
- 59 Hainfeld, J.F., Slatkin, D.N., Focella, T.M., Smilowitz, H.M., 2006, "Gold nanoparticles: a new X-ray contrast agent," *British Journal of Radiology*, Vol. 79, pp. 248-253.
- 60 Eck, W., Craig, G., Sigdel, A., Ritter, G., Old, L.J., Tang, L., Brennan, M.F., Allen, P.J., Mason, M.D., 2008, "PEGylated Gold Nanoparticles Conjugated to Monoclonal F19 Antibodies as Targeted Labeling Agents for Human Pancreatic Carcinoma Tissue," *ACS Nano*, Vol.2, pp. 2263-2272.
- 61 Pilpel, N., 1971, "Metal stearates in pharmaceuticals and cosmetics," *Manuf. Chem. Aerosol News*, Vol. 42, pp. 37-40.
- 62 Mroso, P.V., Li, W.P.O., Irwin, W.J., 1982, "Solid-state stability of aspirin in the presence of excipients: kinetic interpretation, modeling and prediction," *J. Pharm. Sci.*, Vol. 71, pp. 1096-1101.
- 63 Holzer, W., 1983, "An investigation of batch to batch variation of commercial magnesium stearates," *3rd Int. Conf. Pharm. Tech., Paris*, Vol. IV, pp. 72-80.
- 64 Butcher, A.E., Jones, T.M., 1972, "Some physical characteristics of magnesium stearate," *J. Pharm. Pharmacol.*, Vol. 24, pp. 1P-9P.

- 65 Billany, M.R., 1981, "Hydrophobicity of magnesium stearate and its effect on the dissolution rate of a model drug from solid dosage forms," 2nd Int. Conf. Pharm. Tech., Paris, Vol. V, pp. 54-63.
- 66 Moody, G., Rubinstein, M.H., Fitzsimmons, R.A., 1979, "Lubricity measurements of magnesium stearate." J. Pharm. Pharmacol., Vol. 31, pp. 71P.
- 67 Cowley, J.M., 1995, Diffraction physics, Elsevier Science, ISBN 0444822186.
- 68 Kirkland, E., 1998, Advanced computing in Electron Microscopy, Springer, ISBN 0306459361.
- 69 Templeton, A.C., Wuelfing, W.P., Murray, R.W., 2000, Acc. Chem. Res., Vol. 33, pp. 27.
- 70 Crooks, R.M., Zhao, M.Q., Sun, L., Chechik, V., Yeung, L.K., 2001, Acc. Chem. Res., Vol. 34, pp. 181.
- 71 Rolison, D.R., 2003, Science, Vol. 299, pp. 1698.
- 72 Bond, G.C., Thompson, D.T., 2000, Gold Bull., Vol. 33, pp. 41.
- 73 Bond, G.C., 2001, Gold Bull., Vol. 34, pp. 117.
- 74 Klabunde, K.J., Mulukutla, R.S., 2001, Nanoscale Materials in Chemistry, ed. John Wiley & Sons, Inc., New York, pp.223.
- 75 García-Santibañez, F., Barragán-Vidal, A., Gutiérrez, A., Mendoza, M., Ascencio, J.A., 2000, "Experimental and Simulated Analysis of Cu Nanoparticles Produced by Cooled Sample Irradiation." Applied Physics, A Materials Science & Processing, Vol. 71.2, pp. 219.
- 76 Yeh, M.-S., Yang, Y.-S., Lee, Y.-P., Lee, H.-F., Yeh, Y.-H., Yeh, C.-S., 1999, "Formation and Characteristics of Cu Colloids from CuO Powder by Laser Irradiation in 2-Propanol." Journal of Physical Chemistry B, Vol. 103.33, pp. 6851-7.

- 77 Liz-Marzán, Luis M., 2004, "Nanometals: Formation and Color." *Materials Today*, Vol. 7.2, pp. 26-31.
- 78 Miller, T.A., York, P., 1985, *International Journal of Pharmaceutics*, Vol. 23, pp. 55-67.
- 79 Stefan, A.S., Metin, C., Ann, W.N., Harry, G.B., 1997, *Structural Chemistry*, Vol. 8, pp. 73-84.
- 80 Bond, G.C., Thompson, D.T., 2000, *Gold Bull.*, Vol. 33, pp. 41.
- 81 Bond, G.C., 2001, *Gold Bull.*, Vol. 34, pp. 117.
- 82 Klabunde, K.J., Mulukutla, R.S., 2001, *Nanoscale Materials in Chemistry*, ed. John Wiley & Sons, Inc., New York, pp.223.
- 83 García-Santibañez, F., Barragán-Vidal, A., Gutiérrez, A., Mendoza, M., Ascencio, J.A., 2000, "Experimental and Simulated Analysis of Cu Nanoparticles Produced by Cooled Sample Irradiation." *Applied Physics A Materials Science & Processing*, Vol. 71.2, pp. 219.
- 84 Yeh, M.-S., Yang, Y.-S., Lee, Y.-P., Lee, H.-F., Yeh, Y.-H., Yeh, C.-S., 1999, "Formation and Characteristics of Cu Colloids from CuO Powder by Laser Irradiation in 2-Propanol." *Journal of Physical Chemistry B*, Vol. 103.33, pp. 6851-7.
- 85 Liz-Marzán, Luis M., 2004, "Nanometals: Formation and Color." *Materials Today*, Vol. 7.2, pp. 26-31.
- 86 Miller, T.A., York, P., 1985, *International Journal of Pharmaceutics*, Vol. 23, pp. 55-67
- 87 Stefan, A.S., Metin, C., Ann, W.N., Harry, G.B., 1997, *Structural Chemistry*, Vol. 8, pp. 73-84.

List of the symbols and abbreviations

Symbols / Abbreviations	Explanation
IUPAC	International Union of Pure and Applied Chemistry
CAS	Chemical Abstract Service
PAS	Public Available Specifications
PubChem	Database of chemical molecules
TEM	Transmission Electron Microscopy
DTA	Differential Thermal Analysis
TG	Thermogravimetry
SEM	Scanning Electron Microscopy
FTIR	Fourier Transform Infrared Spectroscopy
UV	Ultraviolet-Visible Spectroscopy
HPLC	High Performance Liquid Chromatography
NMR	Nuclear Magnetic Resonance
NP	Nanoparticle
NPs	Nanoparticles
Mg-NPs	magnesium nanoparticles
PEG	Poly(ethylene glycol)
SAMs	self-assembled monolayers
PVP	polyvinyl Pyrrolidone
DMF	Dimethyl formamide
DMSO	dimethyl sulfoxide
Mg	Magnesium
MP	melting point
Cu	Copper
C	Carbon
H	Hydrogen
O	Oxygen

Acknowledgement

I would like to express my heartfelt gratitude and indebtedness to my respected supervisor Professor Dr. Mohammad Abu Yousuf, Department of chemistry, Khulna University of Engineering and Technology, Khulna, for his constant guidance, keen supervision, invaluable suggestion and encouragement throughout the course of this research work.

I would also like to express my gratitude to Dr. Md. Abdul Aziz, Professor & Head, Department of chemistry, KUET, Khulna. I would also like to express my appreciation to Dr. Md. Abdul Motin, Dr. Md. Mizanur Rahman Badal, Mr. Md. Elius Hossain, and other faculty members of this department.

I would like to express my profound appreciation to Dr. M A Kader, CEO, Viola Vitalis, Mohakhali, Dhaka, Bangladesh for giving me a lot of experimental support through his company.

I am obliged to my teacher Professor Dr. Md. Rabiul Islam, Department of chemistry, Jahangirnagar University, Savar, Dhaka for his important instructions to research.

I would like to thank Mr. Md. Joinal Abedin, Senior Demonstrator, and other staff, Department of Chemistry, KUET, Khulna. All of them helped me according to their ability.

I would also like to thank Md. Moniruzzaman, an M. Phil. student of this department, who helped me a lot in writing my thesis. I would like to thank my friends and all colleagues for their continuous support throughout my research work.

Thanks to my better half Shahana Parvin who actually suffered most during this work. She inspired me all the while and gave all sorts of family support in this time.

Finally, special thanks to the members of governing body of Rupsha Degree College, Rupsha, Khulna and to *Shaikh Abdus Sattar*, Principal of the same. They gave me constant official and mental support and opportunity to complete the research works. I will never forget such an enormous, institutional co-operation.

Md. Hafizur Rahman